

1 **Biomass burning emissions and potential air quality impacts of**
2 **volatile organic compounds and other trace gases from fuels**
3 **common in the United States**

4
5 **J.B. Gilman^{1,2}, B.M. Lerner^{1,2}, W.C. Kuster^{1,2*}, P.D. Goldan^{1,2*}, C. Warneke^{1,2}, P.R. Veres^{1,2},**
6 **J.M. Roberts², J.A. de Gouw^{1,2}, I.R. Burling^{3**}, and R.J. Yokelson³**

7
8 [1] CIRES at University of Colorado, Boulder, CO

9 [2] NOAA Earth System Research Laboratory, Boulder, CO

10 [3] Department of Chemistry, University of Montana, Missoula, Montana, USA

11 [*] Now retired

12 [**] Now with Cytec Canada, Niagara Falls, Ontario, Canada

13 Correspondence to: Jessica.Gilman@NOAA.gov

14
15 **Abstract**

16 A comprehensive suite of instruments was used to quantify the emissions of over 200 organic
17 gases, including methane and volatile organic compounds (VOCs), and 9 inorganic gases from 56
18 laboratory burns of 18 different biomass fuel types common in the southeastern, southwestern, or
19 northern United States. A gas chromatograph-mass spectrometry (GC-MS) instrument provided
20 extensive chemical detail of discrete air samples collected during a laboratory burn and was
21 complemented by real-time measurements of organic and inorganic species via an open-path Fourier
22 transform infrared spectroscopy (OP-FTIR) instrument and 3 different chemical ionization-mass
23 spectrometers. These measurements were conducted in February 2009 at the U.S. Department of
24 Agriculture's Fire Sciences Laboratory in Missoula, Montana and were used as the basis for a number of
25 emission factors reported by Yokelson et al. (2013). The relative magnitude and composition of the
26 gases emitted varied by individual fuel type and, more broadly, by the 3 geographic fuel regions being
27 simulated. Discrete emission ratios relative to carbon monoxide (CO) were used to characterize the
28 composition of gases emitted by mass; reactivity with the hydroxyl radical, OH; and potential secondary
29 organic aerosol (SOA) precursors for the 3 different U.S. fuel regions presented here. VOCs contributed
30 less than $0.78\% \pm 0.12\%$ of emissions by mole and less than $0.95\% \pm 0.07\%$ of emissions by mass (on
31 average) due to the predominance of CO₂, CO, CH₄, and NO_x emissions; however, VOCs contributed 70-
32 90 ($\pm 16\%$) to OH reactivity and were the only measured gas-phase source of SOA precursors from
33 combustion of biomass. Over 82% of the VOC emissions by mole were unsaturated compounds
34 including highly reactive alkenes and aromatics and photolabile oxygenated VOCs (OVOCs) such as
35 formaldehyde. OVOCs contributed 57-68% of the VOC mass emitted, 41-54% of VOC-OH reactivity, and
36 aromatic-OVOCs such as benzenediols, phenols, and benzaldehyde were the dominant potential SOA
37 precursors. In addition, ambient air measurements of emissions from the Fourmile Canyon Fire that

38 affected Boulder, Colorado in September 2010 allowed us to investigate biomass burning (BB) emissions
39 in the presence of other VOC sources (i.e., urban and biogenic emissions) and identify several promising
40 BB markers including benzofuran, 2-furaldehyde, 2-methylfuran, furan, and benzonitrile.

41 **Keywords:** Biomass burning, emissions, VOCs, OH reactivity, SOA potential

42 1 Introduction

43 Biomass burning (BB) emissions are composed of a complex mixture of gases and particles that
44 may directly and/or indirectly affect both climate and air quality (Jaffe and Wigder, 2012; Sommers et al.,
45 2014). Emissions include greenhouse gases such as carbon dioxide (CO₂), methane (CH₄), and nitrous
46 oxide (N₂O); carcinogens such as formaldehyde and benzene; and other components potentially harmful
47 to human health including particulate matter, carbon monoxide (CO) and isocyanic acid (HNCO) (Crutzen
48 and Andreae, 1990; Hegg et al., 1990; Andreae and Merlet, 2001; Demirbas and Demirbas, 2009;
49 Estrellan and Iino, 2010; Roberts et al., 2010; Roberts et al., 2011; Sommers et al., 2014). The co-
50 emission of nitrogen oxides (NO_x = NO + NO₂) and reactive volatile organic compounds (VOCs, also
51 known as non-methane organic compounds) from combustion of biomass may degrade local and regional
52 air quality by the photochemical formation of tropospheric ozone (O₃), a hazardous air pollutant, and
53 secondary organic aerosol (SOA) (Alvarado et al., 2015). This work characterizes primary biomass
54 burning emissions of organic and inorganic gases of fuels common to the United States and compares
55 the relative impacts on regional air quality as it relates to potential O₃ and SOA formation.

56 Tropospheric O₃ may be formed in the atmosphere from the interactions of VOCs, NO_x, and a
57 radical source such as the hydroxyl radical (OH), which is formed from the photolysis of O₃, aldehydes,
58 hydroperoxides, or nitrous acid (HONO). Biomass burning is a large, primary source of VOCs, NO_x, and
59 HONO (i.e., O₃ precursors); however, these species are emitted at varying relative ratios depending on
60 the fuel type and burn conditions making it difficult to predict O₃ formation from the combustion of
61 biomass (Akagi et al., 2011; Jaffe and Wigder, 2012). An additional O₃ formation pathway occurs via
62 oxidation of VOCs often initiated by reaction with the hydroxyl radical (-OH) in the presence of NO₂
63 leading to the formation of peroxy nitrates, such as peroxyacetic nitric anhydride (PAN). The formation of
64 peroxy nitrates may initially diminish O₃ formation in fresh BB plumes due to the initial sequestration of
65 NO₂, but enhance O₃ downwind formation via production of NO₂ from thermal dissociation of
66 peroxy nitrates (Jaffe and Wigder, 2012). Due to the complex relationship between O₃ production and
67 VOC/NO_x ratios and peroxy nitrates, we use OH reactivity as a simplified metric to compare reactivity of all
68 measured gaseous emissions by fuel region in order to identify the key reactive species that may
69 contribute to photochemical O₃ formation.

70 SOA is organic particulate mass that is formed in the atmosphere from the chemical evolution of
71 primary emissions of organic species. Here, chemical evolution refers to a complex series of reactions of
72 a large number of organic species that results in the formation of relatively low volatility and/or high
73 solubility oxidation products that will readily partition to, or remain in, the particle phase (Kroll and
74 Seinfeld, 2008). SOA formation from BB emissions is highly variable (Hennigan et al., 2011) and
75 chemical modeling results suggest that there is a “missing large source of SOA” precursors that cannot
76 be explained by the sum of measured aerosol yields of SOA precursors such as toluene (Alvarado et al.,
77 2015). Aerosol yield is a measure of the mass of condensable compounds created from oxidation per
78 mass of VOC precursor and is often used to predict potential SOA mass of complex mixtures; however,

79 care must be taken to ensure that the aerosol yields for all precursors were determined under similar
80 conditions (e.g., VOC:NO_x ratios, oxidant concentrations, etc.). In order to conduct comparisons of the
81 potential to form SOA on a consistent scale, we use a model-based unitless metric, termed SOA potential
82 (SOAP), published by Derwent et al. (2010) which “reflects the propensity of VOCs to form SOA on an
83 equal mass basis relative to toluene.”

84 Advances in instrumentation and complementary measurement approaches have enabled
85 chemical analyses of a wide range of species emitted during laboratory-based biomass burning
86 experiments (Yokelson et al., 1996; McDonald et al., 2000; Schauer et al., 2001; Christian et al., 2003;
87 Veres et al., 2010; Yokelson et al., 2013; Hatch et al., 2015; Stockwell et al., 2015). This information
88 supplements several decades of field measurements of BB emissions reported in the literature (Andreae
89 and Merlet, 2001; Friedli et al., 2001; Akagi et al., 2011; Simpson et al., 2011). Chemically detailed,
90 representative measurements of VOCs and other trace gases from biomass combustion are critical input
91 to photochemical transport models aimed at reproducing observed downwind changes in the
92 concentrations of reactive species including VOCs, O₃, peroxy nitrates, and organic aerosol (Trentmann et
93 al., 2003; Trentmann et al., 2005; Mason et al., 2006; Alvarado and Prinn, 2009; Heilman et al., 2014;
94 Urbanski, 2014; Alvarado et al., 2015) and are essential to understanding impacts on chemistry, clouds,
95 climate, and air quality.

96 For this study, a comprehensive suite of gas-phase measurement techniques was used to
97 quantify the emissions of 200 organic gases, including methane and VOCs, and 9 inorganic gases from
98 laboratory biomass burns of 18 fuel types from 3 geographic regions in the US (hereafter referred to as
99 “fuel regions”) in order to compare the potential atmospheric impacts of these gaseous emissions. A list
100 of all gas-phase instruments and manuscripts detailing the results of the coincident measurement
101 techniques is included in Table 1. These companion manuscripts include fire-integrated ERs for species
102 such as inorganic gases including HONO (Burling et al., 2010) and HNCO (Roberts et al., 2010), organic
103 acids (Veres et al., 2010), formaldehyde and methane (Burling et al., 2010), and a large number of
104 identified and unidentified protonated molecules (Warneke et al., 2011). Yokelson et al. (2013)
105 synthesized the results of all the measurement techniques, including the GC-MS data presented here, in
106 an effort to compile an improved set of fuel-based emission factors for prescribed fires by coupling lab
107 and field work. Comparisons between laboratory and field measurements of BB emission factors are
108 presented elsewhere (Burling et al., 2010; Burling et al., 2011; Yokelson et al., 2013).

109 Here we detail the results of the 56 biomass burns sampled by a gas chromatography-mass
110 spectrometry (GC-MS) instrument which provided unparalleled chemical speciation, but was limited to
111 sampling a relatively short, discrete segment of a laboratory burn. We begin by comparing mixing ratios
112 measured by the GC-MS instrument to those concurrently measured by infrared spectroscopy and
113 proton-transfer-reaction mass spectrometry, both of which provide high time resolution sampling of
114 laboratory fires. We then compare discrete ERs and fire-integrated ERs, representing the entirety of
115 emissions from a laboratory burn, in order to quantify any potential bias that resulted from discrete versus

116 “continuous” sampling techniques utilized in this study. In order to merge datasets from multiple
117 instruments, we report mean discrete emission ratios (ER) of over 200 identified gases relative to CO for
118 southwestern, southeastern, and northern fuel regions to compare the chemical composition of the mass
119 emitted, the reactivities of the measured gases with the hydroxyl radical in order to identify the key
120 reactive species that will likely contribute to O₃ formation, and utilize a model-derived metric developed by
121 Derwent et al. (2010) to compare relative SOA formation potentials from each fuel region. Detailed
122 chemical models are required to more accurately account for the various O₃ and SOA formation
123 pathways, which is beyond the scope of this study.

124 In addition to the laboratory fire measurements, we present field-measurements of rarely-reported
125 VOCs in ambient air during the Fourmile Canyon Fire that affected Boulder, Colorado in September 2010.
126 The latter measurements revealed BB markers that were specific to the BB emissions, minimally
127 influenced by urban or biogenic VOC emission sources, and were emitted in detectable quantities with
128 long enough lifetimes to be useful even in aged, transported BB plumes.

129

130 **2 Methods**

131 **2.1 Fuel and biomass burn descriptions**

132 The laboratory-based measurements of BB emissions were conducted in February 2009 at the
133 U.S. Department of Agriculture’s Fire Sciences Laboratory in Missoula, Montana. A detailed list of the
134 biomass fuel types, species names, fuel source origin, and the carbon and nitrogen content of the fuels
135 studied here are included in Burling et al. (2010). Up to 5 replicate burns were conducted for each of the
136 18 different fuels studied. These fuels are categorized into 3 geographic fuel regions based on where the
137 fuels were collected. The data presented here include 9 southwestern fuels from southern California and
138 Arizona including chaparral shrub, mesquite, and oak savanna/woodland; 6 southeastern fuels
139 represented the pine savanna/shrub complexes indigenous to coastal North Carolina and pine litter from
140 Georgia; and 3 northern fuels including an Englemann spruce, a grand fir, and ponderosa pine needles
141 from Montana. All fuels were harvested in January 2009 and sent to the Fire Sciences Laboratory where
142 they were stored in a walk-in cooler prior to these experiments.

143 All biomass burns were conducted inside the large burn chamber (12.5 x 12.5 x 20 m height),
144 which contains a fuel bed under an emissions-entraining hood, an exhaust stack, and an elevated
145 sampling platform surrounding the exhaust stack approximately 17 m above the fuel bed (Christian et al.,
146 2003; Christian et al., 2004; Burling et al., 2010). Each fuel sample was arranged on the fuel bed in a
147 manner that mimicked their natural orientation and fuel loading when possible and was ignited using a
148 small propane torch (Burling et al., 2010). During each fire, the burn chamber was slightly pressurized
149 with outside air conditioned to a similar temperature and relative humidity as the ambient air inside the
150 burn chamber. The subsequent emissions were entrained by the pre-conditioned ambient air and
151 continuously vented through the top of the exhaust stack. The residence time of emissions in the exhaust

152 stack ranged from ~5 to 17 seconds depending on the flow/vent rate. Each burn lasted approximately 20-
153 40 min from ignition to natural extinction.

154 **2.2 Instrumentation and sampling**

155 A list of the gas-phase instruments and measurement techniques used in this study, a brief
156 description of the inherent detection qualifications of each instrument, and references appears in Table 1.
157 The gas chromatography-mass spectrometry (GC-MS) instrument and the proton-transfer-reaction mass
158 spectrometry (PTR-MS) instrument were located in a laboratory adjacent to the burn chamber. The
159 proton-transfer-reaction ion-trap mass spectrometry (PIT-MS) instrument, negative-ion proton-transfer
160 chemical-ionization mass spectrometry (NI-PT-CIMS) instrument, and open-path Fourier transform
161 infrared (OP-FTIR) optical spectroscopy instrument were located on the elevated platform inside the burn
162 chamber. Hereafter, each instrument will be referred to by the associated instrument identifier listed in
163 Table 1.

164 Sampling inlets for the four mass spectrometers were located on a bulkhead plate on the side of
165 the exhaust stack 17 m above the fuel bed. The GC-MS and PTR-MS shared a common inlet, which
166 consisted of 20 m of unheated 3.97 mm i.d. perfluoroalkoxy Teflon tubing (Warneke et al., 2011). The
167 portion of the inlet line inside the exhaust stack (40 cm) was sheathed by a stainless steel tube (40 cm,
168 6.4 mm I.D) that extended 30 cm from the wall of the exhaust stack and was pointing upwards (away from
169 the fuel bed below) in an effort to reduce the amount of particles pulled into the sample line. A sample
170 pump continuously flushed the 20 m sample line with 7 L min^{-1} flow of stack air reducing the inlet
171 residence time to less than 3 seconds. Separate inlets for both the PIT-MS and NI-PT-CIMS were of
172 similar materials and design, but shorter lengths further reducing inlet residence times and allowing for
173 sample dilution for the NI-PT-CIMS (Roberts et al., 2010; Veres et al., 2010).

174 The open optical path of the OP-FTIR spanned the full width of the exhaust stack so that the
175 emissions could be measured instantaneously without the use of an inlet. All measurements were time
176 aligned with the OP-FTIR in order to account for different inlet residence times and instrument response
177 times. Previous comparisons of OP-FTIR to a PTR-MS with a moveable inlet confirmed the stack
178 emissions are well-mixed at the height of the sampling platform (Christian et al., 2004). Other possible
179 sampling artifacts, such as losses to the walls of the inlets, were investigated via laboratory tests and in-
180 situ instrument comparisons (Burling et al., 2010; Roberts et al., 2010; Veres et al., 2010; Warneke et al.,
181 2011).

182 **2.3 Discrete sampling by in-situ GC-MS**

183 A custom-built, dual-channel GC-MS was used to identify and quantify an extensive set of VOCs.
184 For each biomass burn, the GC-MS simultaneously collected two samples, one for each channel, and
185 analyzed them in series using either an $\text{Al}_2\text{O}_3/\text{KCl}$ PLOT column (channel 1) or a semi-polar DB-624
186 capillary column (channel 2) plumbed to a heated 4-port valve that sequentially directed the column
187 effluent to a linear quadrupole mass spectrometer (Agilent 5973N). The sample traps for each channel
188 were configured to maximize the cryogenic trapping efficiencies of high-volatility VOCs (channel 1) or

189 VOCs of lesser volatility and/or higher polarity (channel 2) while minimizing the amount of CO₂ and water
190 in each sample (Goldan et al., 2004; Gilman et al., 2010). While ozone traps were not required for these
191 experiments, they were left in the sample path in order to be consistent with other ambient air
192 measurements and laboratory calibrations using this instrument.

193 For each channel, 70 mL min⁻¹ was continuously sub-sampled from the high volume (7 L min⁻¹)
194 sample stream for 20 to 300 seconds resulting in sample volumes from 23-350 mL each. Smaller sample
195 volumes were often collected during periods of intense flaming combustion in order to avoid trapping
196 excessive CO₂, which could lead to dry ice forming in the sample trap, thereby restricting sample flow.
197 Larger sample volumes allowed for detection of trace species, but peak resolution would degrade if the
198 column was overloaded. Sample acquisition times longer than 300 seconds were not possible with the
199 GC-MS used in this study.

200 The mass spectrometer was operated in either total ion mode, scanning all mass-to-charge ratios
201 (*m/z*) from 29 to 150; or in selective ion mode, scanning a subset of *m/z*'s. The majority of the samples
202 were analyzed in selective ion mode for improved signal-to-noise; however, at least one sample of each
203 fuel type was analyzed in total ion mode to aid identification and quantify species whose *m/z* may not
204 have been scanned in selective ion mode. The entire GC-MS sampling and analysis cycle required 30
205 minutes; therefore, the GC-MS was limited to sampling each laboratory burn only once per fire for burns
206 that lasted less than 30 minutes. GC-MS samples were collected at different stages of replicate burns, as
207 determined by visual inspection of the fire in addition to the real-time measurements via PTR-MS, in an
208 effort to best characterize the emissions of each fuel type.

209 Each VOC was identified by its retention time and quantified by the integrated peak area of a
210 distinctive *m/z* in order to reduce any potential interferences from co-eluting compounds. Identities of
211 new compounds that had never before been measured by this GC-MS were confirmed by 1) matching the
212 associated electron ionization mass spectrum when operated in total ion mode to the National Institute of
213 Standards and Technology's mass spectral database, and 2) comparing their respective retention times
214 and boiling points to a list of compounds previously measured by the GC-MS. Examples of these species
215 include: 1,3-butadiyne (C₄H₂), butenyne (vinyl acetylene, C₄H₄), methyl nitrite (CH₃ONO), nitromethane
216 (CH₃NO₂), methyl pyrazole (C₄H₆N₂), ethyl pyrazine (C₆H₈N₂), and tricarbon dioxide (carbon suboxide,
217 C₃O₂). For some species, we were able to identify the chemical family (defined by its molecular formula
218 and common chemical moiety) but not the exact chemical structure or identity. For these cases, we
219 present the emissions as a sum of the unidentified isomers for a particular chemical family (see Table 2).
220 We report only the compounds that were above the limits of detection for the majority of the biomass
221 burns and where the molecular formula could be identified.

222 Of the 187 gases quantified by the GC-MS in this study, 95 were individually calibrated with
223 commercially available and/or custom-made gravimetrically-based compressed gas calibration standards.
224 The limit of detection, precision, and accuracy are compound dependent, but are conservatively better
225 than 0.010 ppbv, 15%, and 25%, respectively (Gilman et al., 2009; Gilman et al., 2010). For compounds

226 where a calibration standard was not available (identified by an asterisk in Table 2), the calibration factors
 227 were estimated using measured calibrations of compounds in a similar chemical family with a similar
 228 retention time, and when possible a similar mass fragmentation pattern. In order to estimate the
 229 uncertainty in the accuracy of un-calibrated species, we use measured calibrations of ethyl benzene, o-
 230 xylene, and the sum of m- and p-xyles as a test case. These aromatic species have similar mass
 231 fragmentation patterns, are all quantified using *m/z* 91, and elute within 1 minute of each other signifying
 232 similar physical properties. If a single calibration factor was used for all these isomers, then the reported
 233 mixing ratios could be miscalculated by up to 34%. We therefore conservatively estimate the accuracy of
 234 all un-calibrated species as 50%.

235 **2.4 Calculations**

236 **2.4.1 Emission ratios**

237 Emission ratios (ER) to carbon monoxide (CO) for each gas-phase compound, *X*, were calculated
 238 as follows:

$$239 ER = \frac{\Delta X}{\Delta CO} = \frac{\int_{t_{start}}^{t_{end}} (X_{fire} - X_{bknd}) dt}{\int_{t_{start}}^{t_{end}} (CO_{fire} - CO_{bknd}) dt} \quad (1)$$

240 where ΔX and ΔCO are the excess mixing ratios of compound *X* or *CO*, respectively, during a fire above
 241 the background. Background values, X_{bknd} and CO_{bknd} , are equal to the average mixing ratio of a species
 242 in the pre-conditioned ambient air inside the exhaust stack in the absence of a fire. For the OP-FTIR,
 243 PTR-MS, PIT-MS and NI-PT-CIMS, backgrounds were determined from the mean responses of the
 244 ambient air inside the exhaust stack for a minimum of 60 s prior to the ignition of each fire. At least one
 245 background sample was collected for the GC-MS each day. The composition and average mixing ratios
 246 of VOCs in the stack backgrounds were consistent over the course of the campaign and were generally
 247 much lower than the mixing ratios observed during biomass burns. For example, the average
 248 background ethyne measured by the GC-MS was 1.22 ± 0.33 ppbv (median = 1.21 ppbv) compared to a
 249 mean ethyne of 150 ± 460 ppbv (median = 42 ppbv) in the fires. The large standard deviation for ethyne
 250 in the biomass burns reflects the large variability in ethyne emissions rather than uncertainty in the
 251 measurement.

252 The type of emission ratio, discrete or fire-integrated, is determined by the sampling frequency of
 253 the instrument and sampling duration. The GC-MS used in these experiments is only capable of
 254 measuring discrete ERs, which represent the average ΔX relative to ΔCO for a relatively short portion of a
 255 fire corresponding to the GC-MS sample acquisition time. The OP-FTIR, PTR-MS, and NI-PT-CIMS are
 256 fast-response instruments that sampled every 1 to 10 seconds over the entire duration of each fire.
 257 These measurements were used to calculate both fire-integrated ERs that represent to $\Delta X/\Delta CO$ over the
 258 entirety of a fire ($dt \geq 1000$ s) (Burling et al., 2010; Veres et al., 2010; Warneke et al., 2011) as well as
 259 discrete ERs coincident with the GC-MS sample acquisition ($dt = 20$ to 300s) as discussed in Section 2.3.
 260 We reference all ERs to CO because the majority of VOCs and CO are co-emitted by smoldering
 261 combustion during the fire whereas CO₂ emissions occur mostly from flaming (see Section 3.1).

262 Additionally, ratios to CO are commonly reported in the literature for biomass burning and urban VOC
 263 emission sources. All data presented here are in units of ppbv VOC per ppmv CO, which is equivalent to
 264 a molar ratio (mmol VOC per mol CO).

265 **2.4.2 Modified combustion efficiency**

266 Modified combustion efficiency (MCE) is used here to describe the relative contributions of
 267 flaming and smoldering combustion and is equal to:

$$268 \quad MCE = \frac{\Delta CO_2}{[\Delta CO + \Delta CO_2]} \quad (2)$$

269 where ΔCO and ΔCO_2 are the excess mixing ratios of CO or CO_2 , respectively, during a fire above the
 270 background (Yokelson et al., 1996). MCE can be calculated instantaneously or for discrete (time-
 271 integrated) samples.

272 **2.4.3 Degree of unsaturation**

273 The degree of unsaturation (D) is also known as “ring and double bond equivalent” (Murray et al.,
 274 2013) and is equal to:

$$275 \quad D = \frac{[2C+N-H+2]}{2} \quad (3)$$

276 where C, N, and H denote the number of carbon, nitrogen, and hydrogen atoms, respectively. Table 2
 277 includes D values for each species reported.

278 **2.4.4 Molar mass**

279 Molar mass ($\mu g m^{-3}$) emitted per ppmv CO is equal to:

$$280 \quad Molar Mass = \sum \left(\frac{ER \times MW}{MV} \right) \quad (4)$$

281 where ER is the mean discrete emission ratio of a gas, MW is molecular weight ($g mol^{-1}$), and MV is molar
 282 volume (24.5 L at 1 atm and 25°C). Table 2 includes the nominal MW for each species reported.

283 **2.4.5 OH reactivity**

284 Total OH reactivity represents the sum of all sinks of the hydroxyl radical ($\cdot OH$) with all reactive
 285 gases and is equal to:

$$286 \quad OH reactivity = \sum (ER \times k_{OH} \times A) \quad (5)$$

287 where ER is the discrete emission ratio for each measured gases (VOCs, CH_4 , CO, NO_2 , and SO_2 ; ppbv
 288 per ppmv CO), k_{OH} is the second-order reaction rate coefficient of a gas with the hydroxyl radical (cm^3
 289 $molec^{-1} s^{-1}$), and A is a molar concentration conversion factor ($2.46 \times 10^{10} molec cm^{-3} ppbv^{-1}$ at 1 atm and
 290 25°C). Table 2 includes the k_{OH} values for all reported species which were compiled using the National
 291 Institute of Standards and Technology’s Chemical Kinetics Database and the references therein (Manion
 292 et al., 2015). We estimated k_{OH} values (indicated by an asterisk in Table 2) that were not in the database
 293 using those of analogous compounds.

294 **2.4.6 SOA formation potential**

295 The total SOA formation potential represents the sum of all “potential” SOA formed from all
 296 measured gases and is equal to:

$$297 \quad SOA \text{ formation potential} = \sum (ER \times SOAP) \quad (6)$$

298 where *ER* is the discrete emission ratio for each measured gases (VOCs, CH₄, CO, NO₂, and SO₂; ppbv
 299 per ppmv CO) and *SOAP* is a unitless, model-derived SOA potential published by Derwent et al. (2010).
 300 Briefly, Derwent et al. (2010) calculated SOAPs of 113 VOCs using a photochemical transport model that
 301 included explicit chemistry from the Master Chemical Mechanism (MCM v 3.1) and was initialized using
 302 an idealized set of atmospheric conditions typical of a polluted urban boundary layer. All SOAP values
 303 reflect the simulated mass of aerosol formed per mass of VOC reacted and are expressed relative to
 304 toluene (i.e., SOAP_{Toluene} ≡ 100). The SOAP values published in the Derwent et al. (2010) study are
 305 included in Table 2 and were used to estimate values for all other species (indicated by an asterisk in
 306 Table 2) based on chemical similarities. For example, species such as styrene and benzaldehyde have
 307 SOAP values of ~200 (i.e., twice as much potential SOA formed compared to toluene) and were used as
 308 proxies for SOAP values for aromatics with unsaturated substituents, benzofurans, and benzenediols.

309 **2.5 Fourmile Canyon Fire in Boulder, Colorado**

310 Ambient air measurements of biomass burning emissions from the Fourmile Canyon Fire that
 311 occurred in the foothills 10 km west of Boulder, Colorado were conducted from 7-9 September 2010.
 312 Over the course of the Fourmile Fire, approximately 25 km² of land including 168 structures burned. The
 313 burned vegetation consisted primarily of Douglas-fir (*Pseudotsuga menziesii*) and ponderosa pine (*Pinus*
 314 *ponderosa*) mixed with juniper (*Juniperus scopulorum* and *communis*), mountain mahogany
 315 (*Cercocarpus*), and various shrubs and grasses common to the mountain zone of the Colorado Front
 316 Range (Graham et al., 2012). During the measurement period, down-sloping winds ranging from 1 to 12
 317 m s⁻¹ (mean = 3.5 m s⁻¹) periodically brought biomass burning emissions to NOAA’s Earth Systems
 318 Research Laboratory located at the western edge of the city of Boulder. The previously described in-situ
 319 GC-MS was housed inside the laboratory and sampled outside air via a 15 m perfluoroalkoxy Teflon
 320 sample line (residence time < 2 s) attached to an exterior port on the western side of the building. CO
 321 was measured via a co-located vacuum-UV resonance fluorescence instrument (Gerbig et al., 1999).
 322

323 **3 Results and Discussion**

324 **3.1 Temporal profiles and measurement comparisons**

325 Temporal profiles of laboratory biomass burns provide valuable insight into the combustion
 326 chemistry and processes that lead to the emissions of various species (Yokelson et al., 1996). Figure 1
 327 shows temporal profiles of an example burn in order to illustrate (i) flaming, mixed, and smoldering
 328 combustion phases/processes and (ii) the sampling frequencies and temporal overlap of the fast-
 329 response instruments compared to the GC-MS. Upon ignition, there is an immediate and substantial
 330 increase in CO₂ and NO_x (NO + NO₂) indicative of vigorous flaming combustion. This transitions to a
 331 mixed-phase characterized by diminishing CO₂ and NO_x emissions and a second increase in CO. The

332 fire eventually evolves to a weakly-emitting, protracted period of mostly smoldering combustion (Yokelson
333 et al., 1996; Burling et al., 2010). Figure 1 also includes the temporal profile of the modified combustion
334 efficiency (MCE, Eq. (2)) which is a proxy for the relative amounts of flaming and smoldering combustion
335 (Yokelson et al., 1996). During the initial flaming phase of the fire, the MCE approaches unity due to the
336 dominance of CO₂ emissions. The MCE gradually decreases during smoldering combustion when CO
337 emissions are more prominent.

338 In order to compare measurements from multiple instruments, we calculated the average excess
339 mixing ratios of a species, ΔX , measured by the fast-response instruments over the corresponding GC-
340 MS sample acquisition times for all 56 biomass burns. We compare the measurements using correlation
341 plots of ΔX for VOCs measured by the GC-MS versus the same compound measured by the OP-FTIR or
342 an analogous *m/z* measured by the PTR-MS. The slopes and correlation coefficients, *r*, were determined
343 by linear orthogonal distance regression analysis and are compiled in Fig. 2a. The average slope and
344 standard deviation of the instrument comparison is 1.0 ± 0.2 and $0.93 < r < 0.99$ signifying good overall
345 agreement between the different measurement techniques for the species investigated here. A few
346 comparisons are discussed in more detail below.

347 The largest difference between the GC-MS and the OP-FTIR observations was for propene
348 (slope = 1.36) indicating that the GC-MS response is greater than the OP-FTIR; however, a correlation
349 coefficient of 0.99 suggests that the offset is more likely from a calibration difference that remains
350 unresolved. The possibility of a species with the same retention time and similar fragmentation pattern as
351 propene that is also co-emitted at a consistent ratio relative to propene is unlikely, but cannot be
352 completely ruled out. For furan, the GC-MS had a lower response than OP-FTIR (slope = 0.77) indicating
353 that the GC-MS may be biased low for furan or that the OP-FTIR may have spectral interferences that
354 bias the measurement high. The temporal profiles of these measurements shown in Fig. 1 suggest that
355 there was a spectral interference with the OP-FTIR measurement of furan as evidenced by the large
356 emissions in the flaming phase that was not captured by the *m/z* 69 response of the PTR-MS. These
357 early “spurious” OP-FTIR furan responses would (i) only affect the comparison for the GC-MS samples
358 collected in the flaming phase of the fires and (ii) have not been observed in other biomass burning
359 experiments utilizing this OP-FTIR (Christian et al., 2004; Stockwell et al., 2014).

360 Comparison of the GC-MS Σ (isoprene+furan) vs. PTR-MS *m/z* 69 has the lowest slope (GC-MS
361 vs. PTR-MS = 0.64) indicating the contribution of other VOCs, e.g. cis- and trans-1,3-pentadienes, to the
362 *m/z* 69 response of the PTR-MS in fresh smoke (Warneke et al., 2011). Carbon suboxide (C₃O₂) has also
363 been shown to contribute to *m/z* 69 response for the PTR-MS technique (Stockwell et al., 2015). Direct
364 comparisons of the real-time measurements for a variety of other species not measured by the GC-MS
365 (e.g., formaldehyde, formic acid, and HONO) can be found elsewhere (Burling et al., 2010; Veres et al.,
366 2010; Warneke et al., 2011).

367 **3.2 Comparison of discrete and fire-integrated ERs**

368 Fire-integrated ERs represent emissions from all combustion processes of a biomass burn
369 whereas discrete ERs capture a relatively brief snapshot of emissions from mixed combustion processes
370 during a particular sampling period. Figure 1 includes time series of VOC to CO ERs measured by the
371 real-time measurement techniques for select gases. Here we compare the 2 different measurement
372 strategies, discrete vs. fire-integrated, in order to (i) determine if the discrete ERs measured by the GC-
373 MS may be biased by the sample acquisition times which typically occurred within the first-half of a
374 laboratory burn when emissions for most gases generally “peaked” and (ii) assess how well the discrete
375 GC-MS samples are able to capture the fire-to-fire variability of emissions relative to CO. We do this by
376 determining discrete ERs for the OP-FTIR or PTR-MS for each of the 56 biomass burns using Eq. 1
377 where t_{start} and t_{end} times correspond to the GC-MS sample acquisition. The discrete ERs are then
378 compared to the fire-integrated ERs measured by the same fast-response instrument so that potential
379 measurement artifacts will not affect the comparison.

380 The slopes and correlation coefficients, r , of discrete versus fire-integrated ERs for select VOCs
381 are summarized in Fig. 2b. These values were calculated using a linear orthogonal distance regression
382 analysis of correlation plots of discrete vs. fire-integrated ERs as shown in Fig. 3. The average slope and
383 standard deviation is 1.2 ± 0.2 indicating that the discrete ERs are generally higher than the fire-
384 integrated ERs by 20% on average. This positive bias is a consequence of the GC-MS sampling strategy
385 which rarely included samples collected at the end of a burn (e.g., $t \geq 1000$ s in Fig. 1) when absolute
386 emissions and ERs are lower for most species. Using the data in Fig. 1 as an example, 95% of the
387 emissions of benzene (in ppbv) occur between ignition and 1000 s, and the mean ER during this time is
388 twice as large as the mean ER in the later portion of the fire (time = 1001 s to extinction). For VOCs
389 emitted during the later stages of a fire (e.g., 1,3-benzenediol), the discrete ERs will likely underestimate
390 the emissions relative to CO. For example, the discrete ERs for benzenediol for the southeastern and
391 southwestern fuels (Table 2) are 30% lower than the mean fire-integrated ERs reported by Veres et al.
392 (2010).

393 The ability of the GC-MS to capture the fire-to-fire variability in VOC emissions relative to CO is
394 evaluated by the strength of the correlation, r , between the discrete and fire-integrated ERs (Fig. 2b).
395 Species with the weakest correlations, such as ethyne and benzene, show a distinct bifurcation that is
396 dependent upon the MCE of the discrete samples (Fig. 3). These compounds have significant portion of
397 emissions in both the flaming and smoldering phases of a fire (see Fig. 1). For these types of
398 compounds, discrete samples collected in the smoldering phase (low MCE) did not adequately represent
399 the fire-integrated emissions that include the intense flaming emissions (high MCE) resulting in poor
400 correlation between discrete and fire-integrated ERs for these species. In contrast, VOCs that had the
401 strongest correlations between the discrete and fire-integrated ERs (e.g., methanol and toluene where $r >$
402 0.88) do not show a strong dependence on the MCE. Since CO is strongly associated with smoldering
403 combustion (Yokelson et al., 1996; Burling et al., 2010), VOCs emitted primarily during this phase will be
404 more tightly correlated with CO and the variability in the discrete vs. fire-integrated will be minimized.

405 In summary, the discrete GC-MS samples best characterize the fire-integrated emissions and
406 fire-to-fire variability of species produced primarily by smoldering combustion. We conservatively
407 estimate these values to be within a factor of 1.5 of the fire-integrated ERs for the majority of the species
408 measured. A similar conclusion was reached by comparing discrete ERs measured during the same fire
409 to each other by Yokelson et al. (2013). While fire-integrated ERs are considered to best represent BB
410 emissions, these analyses suggest that collecting and averaging multiple discrete ERs at various stages
411 of the same or replicate burns, as presented here, are an adequate substitute when fire-integrated ERs
412 cannot be determined. Fire-integrated ERs are commonly used to determine fuel-based emission factors
413 for a fire, but care must be taken converting discrete ERs into emission factors, as also discussed for this
414 data in Yokelson et al. (2013).

415 **3.3 Characterization of laboratory BB emissions**

416 In order to merge datasets from multiple instruments, we report mean discrete ERs of over 200
417 organic gases, including methane and VOCs, and 9 inorganic gases relative to CO for the southwestern,
418 southeastern, and northern fuel types in the United States (Table 2). Mean ERs for each of the 18
419 individual fuel types are available at <http://www.esrl.noaa.gov/csd/groups/csd7/measurements/2009firelab/>. This study utilizes discrete ERs to characterize the chemical composition of the measured
420 molar mass emitted, the VOC-OH reactivity, and the relative SOA formation potential of the measured
421 gaseous emissions from various fuels categorized by the region where they were collected in order to
422 compare potential atmospheric impacts of these emissions and identify key species that may impact air
423 quality through formation of O₃ and/or SOA.

425 Figure 4 is a pictograph of all ERs presented in Table 2 as well as a histogram of the ERs for
426 each of the 3 fuel regions in order to highlight commonalities and differences in the magnitudes and
427 general chemical composition of fuels from different regions in the U.S.. The distribution of ERs are
428 shown as a function of three simple properties including the degree of unsaturation (D, Eq. (3)); the
429 number of oxygen atoms; and molecular weight (MW) of individual VOCs. Atmospheric lifetimes and
430 fates of VOCs will depend, in part, on these properties, which we use as simplified proxies for reactivity
431 (D), solubility (O-atoms), and volatility (MW). Using this general framework, we highlight several key
432 features that will be explored in further detail in the subsequent sections:

- 433 (i) ERs are highly variable and span more than 4 orders of magnitude.
- 434 (ii) The relative magnitude and composition of the gases emitted are different for fuels from each
435 of the 3 geographic regions, i.e., the distribution of ERs are unique for the fuels within each
436 fuel region.
- 437 (iii) Southwestern fuels generally have lower ERs and northern fuels have the largest ERs.
438 Collectively, the molar emission ratios are a factor of 3 greater for the northern fuels than the
439 southwestern.
- 440 (iv) The largest ERs for all three fuel regions are associated with low molecular weight species
441 (MW < 80 g/mol) and/or those that contain 1 or more oxygen atom(s). These species also

442 have lower degrees of unsaturation ($D \leq 2$) and populate the upper left quadrants of Fig. 4.
 443 VOCs with the largest ERs common to all fuel types are formaldehyde, ethene, acetic acid,
 444 and methanol (Table 2).

445 (v) Over 82% of the molar emissions of VOCs from biomass burning are unsaturated
 446 compounds ($D \geq 1$) defined as having one or more pi-bonds (e.g., C-C or C-O double bonds,
 447 cyclic or aromatic rings, etc.). In general, these species are more likely to react with
 448 atmospheric oxidants and/or photo-dissociate depending on the chemical moiety, making
 449 unsaturated species potentially important O_3 and SOA precursors. VOCs that contain triple
 450 bonds (e.g., ethyne) are a notable exception as they tend to be less reactive.

451 (vi) The number of VOCs in the upper right quadrants of Fig. 4 (increasing ERs and degree of
 452 unsaturation) is greatest for northern fuels and least for southwestern fuels. Many of the
 453 VOCs in this quadrant also have relatively high molecular weights ($MW \geq 100$ g/mol) and
 454 most contain at least one oxygen atom (e.g., benzenediol and benzofuran). The combination
 455 of these physical properties indicate that these species are relatively reactive, soluble, and of
 456 low enough volatility to make them potentially important SOA precursors.

457 **3.3.1 Molar mass of measured emissions**

458 Here we compare the magnitude and composition of biomass burning emissions as a function of
 459 molar mass, which is a readily calculated physical property used to quantify BB emissions. For all 3 fuel
 460 regions, CO_2 was the overwhelmingly dominant gas-phase emission and singularly contributed over 95%
 461 of the molar mass emitted that was measured. Collectively, CH_4 and the inorganic gases (e.g., CO_2 , CO ,
 462 NO_x , etc.) comprised over 99% of all gaseous molar mass emitted and measured, while VOCs
 463 contributed only $0.27 \pm 0.03\%$, $0.34\% \pm 0.03\%$, and $0.95\% \pm 0.07\%$ for the southeastern, southwestern,
 464 and northern fuels, respectively.

465 Figure 5a-c shows the fractional composition and total molar mass of measured VOCs emitted
 466 per ppmv CO for each fuel region. The molar mass emitted by northern fuels ($324 \pm 22 \mu g m^{-3}$ ppmv CO^{-1})
 467 is 3.5 times greater than the southwestern fuels ($92 \pm 9 \mu g m^{-3}$ ppmv CO^{-1}). For all 3 fuel regions, the
 468 emissions are dominated by oxygen-containing VOCs (OVOCs), which collectively comprise 57-68% of
 469 the total mass emissions. The single largest contribution by a single chemical class is from OVOCs with
 470 low degrees of unsaturation ($D \leq 1$), which contribute 29-40% of the total molar mass. This chemical
 471 family is dominated by acetic acid, formaldehyde, and methanol emissions (Table 2). Compared to
 472 hydrocarbons and OVOCs, nitrogen-containing VOCs are emitted in substantially smaller fractions, less
 473 than 8% of the total measured. Dominant nitrogen VOCs include hydrocyanic acid (HCN), isocyanic acid
 474 ($HNCO$), acetonitrile (CH_3CN), and methylnitrite (CH_3ONO). The addition of all nitrogen-containing
 475 organics presented here would add approximately 5% to the nitrogen budget presented in Burling et al.
 476 (2010); however, this would still leave over one-half of the fuel nitrogen potentially ending up in the ash,
 477 or being emitted as N_2 or in other unmeasured gases based on the nitrogen content of the fuels which
 478 ranged from 0.48 to 1.3%.

479 One limitation of this analysis is the exclusion of “unknown” species, which are (i) gaseous
480 compounds that were measured but remain unidentified and were therefore omitted from this analysis
481 because the chemical formula and family could not be properly identified or (ii) were undetectable by the
482 suite of instruments listed in Table 1. We estimate the mass contribution from the first scenario using the
483 fuel-based emission factors compiled by Yokelson et al. (2013) for all measured species including
484 “unknown” masses observed by the PIT-MS. These “unidentified” non-methane organic compounds
485 (NMOC, equivalent to VOCs) accounted for 31-47% of the mass emitted for the same fuels studied here
486 (Yokelson et al., 2013). The second category of un-observed unknown species are likely to be of
487 sufficiently high molecular weight, high polarity, and/or low volatility and thermal stability to escape
488 detection by GC-MS, a variety of chemical ionization mass spectrometers, and the OP-FTIR. For
489 example, BB emissions of species such as glyoxal, glycoaldehyde, acetol, guaiacols, syringols, and
490 amines have been reported in the literature (McDonald et al., 2000; Schauer et al., 2001; McMeeking et
491 al., 2009; Akagi et al., 2011; Akagi et al., 2012; Hatch et al., 2015) but would not be detectable by any of
492 the instruments used in this experiment. The contribution of these types of compounds is difficult to
493 assess, so we roughly estimate an additional contribution of ~ 5% to the total mass of VOCs emitted
494 could be from un-observed unknown VOCs. Collectively, we estimate that the species reported in Table
495 2 and compiled in Fig. 5a-c account for approximately 48-64% of the expected mass of non-methane
496 organic gases emitted from the fuels studied here. The total VOC molar mass for each fuel type should
497 be considered a lower limit and could increase by a factor of ~ 2; however, doubling the molar mass of
498 VOCs to account for all identified and “unknown” species would increase the total mass measured by less
499 than 0.78% since the vast majority of carbon emissions from biomass burning are in the form of CO, CO₂,
500 and CH₄ (Yokelson et al., 1996; Burling et al., 2010). All of the totals presented in Figure 5 should also be
501 considered lower limits; however, the additional contribution of unidentified and/or un-measured species
502 to the following discussions could not be determined.

503 **3.3.2 OH reactivity of BB emissions**

504 Oxidation of VOCs, often initiated by reaction with the hydroxyl radical (·OH), in the presence of
505 NO_x (NO + NO₂) leads to the photochemical formation of O₃ and peroxy nitrates, including peroxyacetic
506 nitric anhydride (PAN). Due to the complex relationship between O₃ production and VOC/NO_x ratios and
507 peroxy nitrates, we use OH reactivity to (i) compare the magnitude of reactive gases emitted by
508 combustion of fuels characteristic of each region and to (ii) identify key reactive species that may
509 contribute to the photochemical formation of O₃ in a BB plume. Based on the calculated OH reactivities of
510 all measured species listed in Table 2, VOCs are the dominant sink of OH for all fuel regions contributing
511 70-90 (\pm 16)% of the total calculated OH reactivity even though non-methane VOCs were only 0.27-0.95%
512 of the molar mass emitted.

513 Figure 5d-f shows the fractional contributions and total VOC-OH reactivities per ppmv CO for
514 each of the 3 fuel regions. The fresh BB emissions from northern fuels have the highest OH reactivity (61
515 \pm 10 s⁻¹ ppmv CO⁻¹), which is 4.7 times greater than southwestern fuels (13 \pm 3 s⁻¹ ppmv CO⁻¹).

516 Collectively, OVOCs provide the majority of the OH reactivity of the southeastern fuels (54%), while
517 hydrocarbons dominate the southwestern (52%) and northern fuels (57%). Northern fuels have the
518 largest contribution from highly reactive terpenes (14%) due to the ERs of these species being, on
519 average, a factor of 5 greater than southeastern fuels and a factor of 40 greater than southwestern fuels.

520 For all 3 fuel regions, alkenes have the largest contribution of any singular chemical class due to
521 the large ERs of the reactive species ethene and propene, the latter of which is the single largest
522 individual contributor to OH reactivity of any species measured. Oxidation of alkenes proceeds by OH
523 addition to the double-bond or hydrogen abstraction and often results in the secondary formation of
524 carbonyls (e.g., acetaldehyde and acetone), which are important peroxy nitrate precursors (Roberts et al.,
525 2007; Fischer et al., 2014). Primary emissions of formaldehyde is the second-largest contributor, after
526 propene, to the OH reactivity of all VOCs emitted for all 3 fuel regions. Formaldehyde is reactive with OH
527 and is a photolytic source of RO[·] radicals that also contribute to O₃ formation, in addition to being an air
528 toxic.

529 Other important contributions to OH reactivity of BB emissions include unsaturated OVOCs (e.g.,
530 2-propenal, methyl vinyl ketone, and methacrolein), poly-unsaturated alkenes (e.g., 1,3-butadiene and
531 1,3-cyclopentadiene), and furans. The majority of these types of species are highly reactive with a variety
532 of oxidants and many of their oxidation products are photochemically active. For example, oxidation of
533 1,3-butadiene results in highly reactive OVOC products including furans and 2-propenal, a precursor of
534 peroxyacrylic nitric anhydride (APAN) (Tuazon et al., 1999). The OH reactivity of furans is dominated by
535 2-methylfuran, 2-furaldehyde (2-furfural), and furan. Alkyl furans (e.g., 2,5-dimethylfuran and 2-
536 ethylfuran) have reaction rate coefficients on the order of $\sim 1 \times 10^{-10} \text{ cm}^3 \text{ molec}^{-1} \text{ s}^{-1}$ at 298K (roughly
537 equivalent to that of isoprene) and the major oxidation products include dicarbonyls (Bierbach et al.,
538 1992, 1995; Alvarez et al., 2009). Up to 27 furan isomers have been identified from the combustion of
539 Ponderosa Pine (Hatch et al., 2015), indicating this is an important class of species that should be further
540 explored in order to better determine their potential contributions to O₃ and SOA formation.

541 Nitrogen-containing VOCs contribute less than 4% of the OH reactivity of all fuels due to the low
542 reactivities of the most abundant emissions, which often contain -C≡N functional groups. Some nitriles,
543 such as acetonitrile (CH₃CN), can have lifetimes on the order of months making these species good
544 markers of long-range transport of BB plumes (Holzinger et al., 1999; de Gouw et al., 2003; de Gouw et
545 al., 2006). Other more reactive nitrogen-containing organics including 2-propenenitrile, benzonitrile, and
546 heterocyclic species such as pyrroles could serve as BB markers of fresh plumes (Friedli et al., 2001; Karl
547 et al., 2007).

548 **3.3.3 SOA formation potential of BB emissions**

549 Figure 5g-i shows the composition and mean SOA formation potentials of VOCs emitted for each
550 of the 3 fuel regions. Southwestern fuels have the lowest SOA potential (480 per ppmv CO) compared to
551 southeastern and northern fuels that have estimated SOAPs 2.7 and 5.1 times greater, respectively.
552 Unsaturated OVOCs are the dominant fraction for all three fuel regions due to the relatively large ERs

553 and SOAPs of benzenediols (sum of 1,2- and 1,3-), benzaldehyde, and phenols. Schauer et al. (2001)
554 reports significant gaseous emissions of benzenediols from combustion of pine in a fireplace and shows
555 that 1,2-benzenediol (o-benzenediol) is the dominant gas-phase isomer while 1,3-benzenediol (m-
556 benzenediol) is primarily associated with the particle phase. The discrete ERs used in this comparison
557 may underestimate the emissions and SOA contribution of several compounds emitted in the later
558 portions of a laboratory burn when emissions of most VOCs and CO were lower as previously discussed
559 (Sect. 3.2).

560 The largest contributions to SOAP from hydrocarbons include aromatics with saturated functional
561 groups (if any) such as benzene and toluene and aromatics with unsaturated substituents as styrene.
562 Traditionally, these are the species that are thought to be the largest contributors to SOA formation from
563 urban emissions (Odum et al., 1997; Bahreini et al., 2012), although predicted SOA is typically much
564 lower than observed in ambient air suggesting that the aerosol yields may be too low or there are
565 additional SOA precursors that remain unaccounted for (de Gouw et al., 2005).

566 Monoterpenes have a very small (<2%) contribution to total SOAP. The calculated SOAPs of
567 monoterpenes are only 20% that of toluene (Derwent et al., 2010). This is in contrast to measured
568 aerosol yields which are approximately 1.7 times higher for monoterpenes compared to toluene (Pandis
569 et al., 1992). As a sensitivity test, we increased the SOAPs of the monoterpenes by a factor of 10
570 bringing the SOAP ratio of monoterpenes to toluene in line with that of measured aerosol yields. This
571 resulted in modest increases in total SOAP of only 2% for SW and 5% for SE fuels. Northern fuels had
572 the largest increase in total SOAP at 16%. With the adjusted monoterpene SOAPs, the fractional
573 contribution of terpenes increased from 1.8% (Fig. 5i) to 15% of the total SOAP while the contribution of
574 unsaturated OVOCs remained the dominant class but was reduced from 67% to 58% of the total SOAP.
575 This sensitivity test suggests that the contributions of monoterpenes are likely underestimated for
576 northern fuels if the SOAP scale is used; however, the largest contributions to SOAP for the northern
577 fuels continues to be from oxygenated aromatics (benzenediols, phenols, and benzaldehyde). For
578 comparison, Hatch et al. (2015) estimated that the SOA mass formed from the combustion of Ponderosa
579 Pine is dominated by aromatic hydrocarbons (45%), terpenes (25%), phenols (9%), and furans (9%);
580 however, their analysis did not include contributions from benzenediols (not measured), benzaldehyde or
581 benzofurans (measured but not included in estimate).

582 **3.4 Field measurements of BB emissions**

583 Here we present field-measurements of VOCs in ambient air during the Fourmile Canyon Fire
584 that affected Boulder, Colorado in September 2010. The in-situ GC-MS measurements are shown in Fig.
585 6 and summarized in Table 3. We were able to identify and quantify a number of VOCs in ambient BB
586 plumes that we had only previously observed in the fire emissions at the Fire Sciences Laboratory.
587 Analysis of BB plumes from the Fourmile Canyon Fire afforded a unique opportunity to investigate BB
588 emissions measured by this same GC-MS system in simulated and real fires and to explore issues
589 associated with the presence of other VOC sources such as urban emissions and natural biogenic

590 emissions during both the daytime and nighttime; with nighttime smoke measurements being very rarely
591 reported (Adler et al., 2011).

592 First we identify the potential emission sources impacting the measurements. Acetonitrile is a
593 common BB tracer that we use to help clarify periods of BB influence. As seen in Fig. 6, BB plumes are
594 readily distinguished by concurrent increases in acetonitrile (CH_3CN), carbon monoxide (CO), and several
595 VOCs. Species such as benzonitrile and furan are very tightly correlated with acetonitrile ($r > 0.94$, Table
596 3) and enhancements in ambient mixing ratios above detection limit only occur in the BB plumes
597 indicating that BB was the only significant source of these compounds. VOCs such as isoprene and
598 alpha-pinene were similarly enhanced in the BB plumes and well correlated with acetonitrile during BB
599 episodes; however, the mixing ratios observed in the BB plume were generally lower than those observed
600 at other times from the natural sunlight-dependent emissions of isoprene (e.g., 09:00 – 15:00 local time)
601 and from the accumulation of monoterpenes in the nocturnal boundary layer (e.g., 9/8/2010 18:00 to
602 9/9/2010 06:00). 3-Carene was the only monoterpene that had significantly higher mixing ratios in the BB
603 plume than in biogenic emissions. Ethene, ethyne, benzene, styrene, and methanol were enhanced in
604 the BB plumes but are also present in urban emissions. An urban plume at 06:00-09:00 9/9/2010 (Fig. 6)
605 is enhanced in all of these species and CO; however, acetonitrile is not enhanced.

606 Observed enhancement ratios of several VOCs relative to acetonitrile and CO are compiled in
607 Table 3 along with the types of emission sources for each VOC. Figure 7 shows a comparison of the
608 VOC to acetonitrile ratios of select species for the Fourmile Canyon Fire and the laboratory-based
609 biomass burns of all fuel types. We have identified benzofuran, 2-furaldehyde, 2-methylfuran, furan, and
610 benzonitrile as the “best” tracers for BB emissions from these observations. These species (i) were well
611 correlated with both acetonitrile and CO in the BB plumes, (ii) had negligible emissions from the urban
612 and biogenic sources impacting the measurement site, and (iii) had large enhancements in BB plumes.
613 In theory, the relative ratios of these species to acetonitrile may also be used as a BB-specific
614 photochemical clock since each of these species represent a range of reactivities that are much greater
615 than that of acetonitrile (Table 3). We compared the enhancement ratios of each VOC marker vs.
616 acetonitrile for the two BB plumes observed on 9/8/2010 in order to determine if the relative age of the
617 two BB plumes could be distinguished. While the enhancement ratios for several VOCs in each plume
618 were statistically different from one another, there was no clear relationship between the observed
619 differences in the enhancement ratios and the relative reactivity of the VOCs. Thus, small differences in
620 the observed enhancement ratios more likely relate to differences in the fuel composition, the relative
621 ratio of flaming vs. smoldering emissions in each BB plume, or variable secondary sources. Given
622 enough time for significant photochemistry to occur as a BB plume moves further from the source, these
623 ratios could be more useful to estimate photochemical ages.

624

625 **4 Conclusions**

626 We report a chemically detailed analysis of the trace gases emitted from burning 18 different
627 biomass fuel types important in the southwestern, southeastern, and northern U.S. A complementary
628 suite of state-of-the-art instruments was used to identify and quantify over 200 organic and 9 inorganic
629 gases emitted from laboratory burns. Most of the species were quantified via discrete sampling by the
630 GC-MS, which also provided confirmation for the real-time PIT-MS and PTR-MS mass assignments
631 (Warneke et al., 2011). The variability in emissions over the course of each biomass burn was measured
632 in detail by the fast-response instruments providing valuable insight into the combustion chemistry and
633 processes that govern the emissions of various species.

634 By comparing discrete and fire-integrated ERs for various VOCs relative to CO, we show that the
635 discrete GC-MS samples adequately represented the fire-integrated ER within an average factor of $1.2 \pm$
636 0.2 and fire-to-fire variability for VOCs emitted mainly by smoldering, which are the majority of VOCs.
637 Discrete ERs for VOCs emitted by both flaming and smoldering were highly variable and showed a clear
638 bifurcation depending on the mix of combustion processes during sampling. This analysis highlights the
639 importance of collecting multiple discrete samples at various stages of replicate burns if fire-integrated
640 emissions cannot be measured to ensure adequate measurement of all VOCs.

641 The distribution of VOC emissions (magnitude and composition) was different for each fuel
642 region. The largest total VOC emissions were from fuels representing the northern U.S. while
643 southwestern U.S. fuels produced the lowest total VOC emissions. VOCs contributed less than $0.78\% \pm$
644 0.12% of total detected gas-phase emissions by mole and less than $0.95\% \pm 0.07\%$ by mass due to the
645 predominance of CO₂, CO, CH₄, and NO_x emissions. However, VOCs contributed 70-90 ($\pm 16\%$) of the
646 total calculated OH reactivity and 100% of the potential SOA precursors emitted from combustion of
647 biomass. Over 82% of the VOC emissions by mole are unsaturated species including highly reactive
648 alkenes, aromatics and terpenes as well as photolabile OVOCs such as aldehydes and ketones. VOCs
649 with the largest ERs common to all fuel types are formaldehyde, ethene, acetic acid, and methanol.

650 OVOCs contributed the dominant fraction of both the total VOC mass emitted (>57%) and
651 potential SOA precursors (>52%), and also contributed a significant fraction of the OH reactivity for all fuel
652 regions making them an important class of VOCs to understand the air quality impacts of BB emissions.
653 Reactive and photolabile OVOCs such as formaldehyde, 2-propenal (acrolein), and 2-butenal
654 (crotonaldehyde) are toxic, a source of free radicals, and/or precursors of peroxy nitrates that may
655 contribute to O₃ formation downwind of the source. Furans are a class of OVOCs in BB emissions that
656 contributed 9 to 14% of the VOC-OH reactivity for all fuel regions; however, their potential as SOA
657 precursors, particularly for species such as 2-furaldehyde and benzofuran, requires further study. The
658 estimated SOA formation potential was dominated by oxygenated aromatics (benzenediols, phenols, and
659 benzaldehyde). Potentially important species that were not measured but should be considered in future
660 studies include glyoxal, glycoaldehyde, acetol, guaiacols, and syringols (Stockwell et al., 2015).

661 The Fourmile Canyon Fire in Boulder, CO, allowed us to identify and quantify a number of VOCs
662 in ambient BB plumes that we had only previously observed in the emissions from laboratory fires at the

663 Fire Sciences facility and investigate BB emissions in the presence of other VOC sources such as urban
664 emissions and biogenic emissions during both the day and nighttime. We identified benzofuran, 2-
665 furaldehyde, 2-methylfuran, furan, and benzonitrile as the “best” tracers for BB emissions from our
666 observations. In theory, the relative ratios of these species to acetonitrile may also be used as a BB-
667 specific photochemical clock since each of these species represent a range of reactivities assuming a
668 negligible photochemical source.

669

670 Acknowledgements

671 This work was supported by the Strategic Environmental Research and Development Program
672 (SERDP) projects RC-1648 and RC-1649 and we thank the sponsors for their support. J. Gilman, W.
673 Kuster, P. Veres, J. M. Roberts, C. Warneke, and J. de Gouw were supported in part by National Science
674 Foundation (NSF) Grant No. ATM 1542457, the CIRES Innovative Research Program, and NOAA’s
675 Health of the Atmosphere and Climate Goals Programs. R. Yokelson was also supported by NSF Grant
676 No. ATM 0936321. We appreciate the efforts of Jim Reardon, David Weise, Joey Chong, Bonni Corcoran,
677 Amy Olson, Violet Holley, Signe Leirfallom, Anna Lahde, Juhn Rawling, Greg Cohen, and Emily Lincoln to
678 sample/harvest the wildland fuels and/or assemble the laboratory fuel beds for this study.

679

680 References

681 Adler, G., Flores, J. M., Riziq, A. A., Borrmann, S., and Rudich, Y.: Chemical, physical, and optical
682 evolution of biomass burning aerosols: a case study, *Atmos. Chem. Phys.*, 11, 1491-1503,
683 doi:10.5194/acp-11-1491-2011, 2011.

684

685 Akagi, S. K., Yokelson, R. J., Wiedinmyer, C., Alvarado, M. J., Reid, J. S., Karl, T., Crounse, J. D., and
686 Wennberg, P. O.: Emission factors for open and domestic biomass burning for use in atmospheric
687 models, *Atmos. Chem. Phys.*, 11, 4039-4072, doi:10.5194/acp-11-4039-2011, 2011.

688

689 Akagi, S. K., Craven, J. S., Taylor, J. W., McMeeking, G. R., Yokelson, R. J., Burling, I. R., Urbanski, S. P.,
690 Wold, C. E., Seinfeld, J. H., Coe, H., Alvarado, M. J., and Weise, D. R.: Evolution of trace gases and
691 particles emitted by a chaparral fire in California, *Atmos. Chem. Phys.*, 12, 1397-1421, doi:10.5194/acp-
692 12-1397-2012, 2012.

693

694 Alvarado, M. J., and Prinn, R. G.: Formation of ozone and growth of aerosols in young smoke plumes
695 from biomass burning: 1. Lagrangian parcel studies, *J. Geophys. Res.-Atmos.*, 114, D09306,
696 doi:10.1029/2008jd011144, 2009.

697

698 Alvarado, M. J., Lonsdale, C. R., Yokelson, R. J., Akagi, S. K., Coe, H., Craven, J. S., Fischer, E. V.,
699 McMeeking, G. R., Seinfeld, J. H., Soni, T., Taylor, J. W., Weise, D. R., and Wold, C. E.: Investigating the
700 links between ozone and organic aerosol chemistry in a biomass burning plume from a prescribed fire in
701 California chaparral, *Atmos. Chem. Phys.*, 15, 6667-6688, doi:10.5194/acp-15-6667-2015, 2015.

702

703 Alvarez, E. G., Borras, E., Viidanoja, J., and Hjorth, J.: Unsaturated dicarbonyl products from the OH-
704 initiated photo-oxidation of furan, 2-methylfuran and 3-methylfuran, *Atmos. Environ.*, 43, 1603-1612,
705 doi:10.1016/j.atmosenv.2008.12.019, 2009.

706

707 Andreae, M. O., and Merlet, P.: Emission of trace gases and aerosols from biomass burning, *Global*
708 *Biogeochem. Cy.*, 15, 955-966, 2001.

709

710 Bahreini, R., Middlebrook, A. M., de Gouw, J. A., Warneke, C., Trainer, M., Brock, C. A., Stark, H., Brown,
711 S. S., Dube, W. P., Gilman, J. B., Hall, K., Holloway, J. S., Kuster, W. C., Perring, A. E., Prevot, A. S. H.,
712 Schwarz, J. P., Spackman, J. R., Szidat, S., Wagner, N. L., Weber, R. J., Zotter, P., and Parrish, D. D.:
713 Gasoline emissions dominate over diesel in formation of secondary organic aerosol mass, *Geophys. Res.*
714 *Lett.*, 39, L06805, doi:10.1029/2011gl050718, 2012.

715

716 Bierbach, A., Barnes, I., and Becker, K. H.: Rate Coefficients For The Gas-Phase Reactions Of Hydroxyl
717 Radicals With Furan, 2-Methylfuran, 2-Ethylfuran And 2,5-Dimethylfuran At 300+/-2-K, *Atmos. Environ.*,
718 26, 813-817, 1992.

719

720 Bierbach, A., Barnes, I., and Becker, K. H.: Product and kinetic study of the oh-initiated gas-phase
721 oxidation of Furan, 2-methylfuran and furanaldehydes at \approx 300 K, *Atmos. Environ.*, 29, 2651-2660,
722 doi:10.1016/1352-2310(95)00096-H, 1995.

723

724 Burling, I. R., Yokelson, R. J., Griffith, D. W. T., Johnson, T. J., Veres, P., Roberts, J. M., Warneke, C.,
725 Urbanski, S. P., Reardon, J., Weise, D. R., Hao, W. M., and de Gouw, J.: Laboratory measurements of
726 trace gas emissions from biomass burning of fuel types from the southeastern and southwestern United
727 States, *Atmos. Chem. Phys.*, 10, 11115-11130, doi:10.5194/acp-10-11115-2010, 2010.

728

729 Burling, I. R., Yokelson, R. J., Akagi, S. K., Urbanski, S. P., Wold, C. E., Griffith, D. W. T., Johnson, T. J.,
730 Reardon, J., and Weise, D. R.: Airborne and ground-based measurements of the trace gases and particles
731 emitted by prescribed fires in the United States, *Atmos. Chem. Phys.*, 11, 12197-12216,
732 doi:10.5194/acp-11-12197-2011, 2011.

733

734 Christian, T. J., Kleiss, B., Yokelson, R. J., Holzinger, R., Crutzen, P. J., Hao, W. M., Saharjo, B. H., and
735 Ward, D. E.: Comprehensive laboratory measurements of biomass-burning emissions: 1. Emissions from
736 Indonesian, African, and other fuels, *J. Geophys. Res.-Atmos.*, 108, doi:10.1029/2003jd003704, 2003.

737

738 Christian, T. J., Kleiss, B., Yokelson, R. J., Holzinger, R., Crutzen, P. J., Hao, W. M., Shirai, T., and Blake, D.
739 R.: Comprehensive laboratory measurements of biomass-burning emissions: 2. First intercomparison of
740 open-path FTIR, PTR-MS, and GC- MS/FID/ECD, *J. Geophys. Res.-Atmos.*, 109, 2004.

741

742 Crutzen, P. J., and Andreae, M. O.: Biomass burning in the Tropics - impact on atmospheric chemistry
743 and biogeochemical cycles, *Science*, 250, 1669-1678, doi:10.1126/science.250.4988.1669, 1990.

744

745 de Gouw, J. A., Warneke, C., Parrish, D. D., Holloway, J. S., Trainer, M., and Fehsenfeld, F. C.: Emission
746 sources and ocean uptake of acetonitrile (CH_3CN) in the atmosphere, *J. Geophys. Res.-Atmos.*, 108,
747 4329, doi:10.1029/2002jd002897, 2003.

748

749 de Gouw, J. A., Middlebrook, A. M., Warneke, C., Goldan, P. D., Kuster, W. C., Roberts, J. M., Fehsenfeld,
750 F. C., Worsnop, D. R., Canagaratna, M. R., Pszenny, A. A. P., Keene, W. C., Marchewka, M., Bertman, S.
751 B., and Bates, T. S.: Budget of organic carbon in a polluted atmosphere: Results from the New England
752 Air Quality Study in 2002, *J. Geophys. Res.-Atmos.*, 110, D16305, doi:10.1029/2004JD005623, 2005.

753

754 de Gouw, J. A., Warneke, C., Stohl, A., Wollny, A. G., Brock, C. A., Cooper, O. R., Holloway, J. S., Trainer,
755 M., Fehsenfeld, F. C., Atlas, E. L., Donnelly, S. G., Stroud, V., and Lueb, A.: Volatile organic compounds
756 composition of merged and aged forest fire plumes from Alaska and western Canada, *J. Geophys. Res.-*
757 *Atmos.*, 111, D10303, doi:10.1029/2005JD006175, 2006.

758

759 Demirbas, M. F., and Demirbas, T.: Hazardous emissions from combustion of biomass, *Energ. Source*, 31,
760 527-534, doi:10.1080/15567030802466953, 2009.

761

762 Derwent, R. G., Jenkin, M. E., Utembe, S. R., Shallcross, D. E., Murrells, T. P., and Passant, N. R.:
763 Secondary organic aerosol formation from a large number of reactive man-made organic compounds,
764 *Sci. Total Environ.*, 408, 3374-3381, doi:10.1016/j.scitotenv.2010.04.013, 2010.

765

766 Estrellan, C. R., and Iino, F.: Toxic emissions from open burning, *Chemosphere*, 80, 193-207,
767 doi:10.1016/j.chemosphere.2010.03.057, 2010.

768

769 Fischer, E. V., Jacob, D. J., Yantosca, R. M., Sulprizio, M. P., Millet, D. B., Mao, J., Paulot, F., Singh, H. B.,
770 Roiger, A., Ries, L., Talbot, R. W., Dzepina, K., and Deolal, S. P.: Atmospheric peroxyacetyl nitrate (PAN): a
771 global budget and source attribution, *Atmos. Chem. Phys.*, 14, 2679-2698, doi:10.5194/acp-14-2679-
772 2014, 2014.

773

774 Friedli, H. R., Atlas, E., Stroud, V. R., Giovanni, L., Campos, T., and Radke, L. F.: Volatile organic trace
775 gases emitted from North American wildfires, *Global Biogeochem. Cy.*, 15, 435-452, 2001.

776

777 Gerbig, C., Schmitgen, S., Kley, D., Volz-Thomas, A., Dewey, K., and Haaks, D.: An improved fast-response
778 vacuum-UV resonance fluorescence CO instrument, *J. Geophys. Res.-Atmos.*, 104, 1699-1704, 1999.

779

780 Gilman, J. B., Kuster, W. C., Goldan, P. D., Herndon, S. C., Zahniser, M. S., Tucker, S. C., Brewer, W. A.,
781 Lerner, B. M., Williams, E. J., Harley, R. A., Fehsenfeld, F. C., Warneke, C., and de Gouw, J. A.:
782 Measurements of volatile organic compounds during the 2006 TexAQS/GoMACCS campaign: Industrial
783 influences, regional characteristics, and diurnal dependencies of the OH reactivity, *J. Geophys. Res.*
784 *Atmos.*, 114, doi:10.1029/2008jd011525, 2009.

785

786 Gilman, J. B., Burkhardt, J. F., Lerner, B. M., Williams, E. J., Kuster, W. C., Goldan, P. D., Murphy, P. C.,
787 Warneke, C., Fowler, C., Montzka, S. A., Miller, B. R., Miller, L., Oltmans, S. J., Ryerson, T. B., Cooper, O.

788 R., Stohl, A., and de Gouw, J. A.: Ozone variability and halogen oxidation within the Arctic and sub-Arctic
789 springtime boundary layer, *Atmos. Chem. Phys.*, 10, 10223-10236, doi:10.5194/acp-10-10223-2010,
790 2010.

791

792 Goldan, P. D., Kuster, W. C., Williams, E., Murphy, P. C., Fehsenfeld, F. C., and Meagher, J.: Nonmethane
793 hydrocarbon and oxy hydrocarbon measurements during the 2002 New England Air Quality Study, *J.*
794 *Geophys. Res.-Atmos.*, 109, D21309, doi:10.1029/2003JD004455, 2004.

795

796 Hatch, L. E., Luo, W., Pankow, J. F., Yokelson, R. J., Stockwell, C. E., and Barsanti, K. C.: Identification and
797 quantification of gaseous organic compounds emitted from biomass burning using two-dimensional gas
798 chromatography-time-of-flight mass spectrometry, *Atmos. Chem. Phys.*, 15, 1865-1899,
799 doi:10.5194/acp-15-1865-2015, 2015.

800

801 Hegg, D. A., Radke, L. F., Hobbs, P. V., Rasmussen, R. A., and Riggan, P. J.: Emissions of some trace gases
802 from biomass fires, *J. Geophys. Res.-Atmos.*, 95, 5669-5675, doi:10.1029/JD095iD05p05669, 1990.

803

804 Heilman, W. E., Liu, Y., Urbanski, S., Kovalev, V., and Mickler, R.: Wildland fire emissions, carbon, and
805 climate: Plume rise, atmospheric transport, and chemistry processes, *Forest Ecol. Manag.*, 317, 70-79,
806 doi:10.1016/j.foreco.2013.02.001, 2014.

807

808 Hennigan, C. J., Miracolo, M. A., Engelhart, G. J., May, A. A., Presto, A. A., Lee, T., Sullivan, A. P.,
809 McMeeking, G. R., Coe, H., Wold, C. E., Hao, W. M., Gilman, J. B., Kuster, W. C., de Gouw, J., Schichtel, B.
810 A., Collett, J. L., Jr., Kreidenweis, S. M., and Robinson, A. L.: Chemical and physical transformations of
811 organic aerosol from the photo-oxidation of open biomass burning emissions in an environmental
812 chamber, 11, 7669-7686, doi:10.5194/acp-11-7669-2011, 2011.

813

814 Holzinger, R., Warneke, C., Hansel, A., Jordan, A., Lindner, W., Scharffe, D. H., Schade, G., and Crutzen,
815 P. J.: Biomass burning as a source of formaldehyde, acetaldehyde, methanol, acetone, acetonitrile, and
816 hydrogen cyanide, *Geophys. Res. Lett.*, 26, 1161-1164, doi:10.1029/1999gl900156, 1999.

817

818 Jaffe, D. A., and Wigder, N. L.: Ozone production from wildfires: A critical review, *Atmos. Environ.*, 51, 1-
819 10, doi:10.1016/j.atmosenv.2011.11.063, 2012.

820

821 Karl, T. G., Christian, T. J., Yokelson, R. J., Artaxo, P., Hao, W. M., and Guenther, A.: The Tropical Forest
822 and Fire Emissions Experiment: method evaluation of volatile organic compound emissions measured by
823 PTR-MS, FTIR, and GC from tropical biomass burning, *Atmos. Chem. Phys.*, 7, 5883-5897,
824 doi:10.5194/acp-7-5883-2007, 2007.

825

826 Kroll, J. H., and Seinfeld, J. H.: Chemistry of secondary organic aerosol: Formation and evolution of low-
827 volatility organics in the atmosphere, *Atmos. Environ.*, 42, 3593-3624,
828 doi:10.1016/j.atmosenv.2008.01.003, 2008.

829

830 Manion, J. A., Huie, R. E., Levin, R. D., Burgess Jr., D. R., Orkin, V. L., Tsang, W., McGivern, W. S.,
831 Hudgens, J. W., Knyazev, V. D., Atkinson, D. B., Chai, E., Tereza, A. M., Lin, C. J., Allison, T. C., Mallard, W.
832 G., Westley, F., Herron, J. T., Hampson, R. F., and Frizzell, D. H.: NIST Standard Reference Database 17,
833 Version 7.0 (Web Version <http://kinetics.nist.gov/>), 2015.

834

835 Mason, S. A., Trentmann, J., Winterrath, T., Yokelson, R. J., Christian, T. J., Carlson, L. J., Warner, T. R.,
836 Wolfe, L. C., and Andreae, M. O.: Intercomparison of two box models of the chemical evolution in
837 biomass-burning smoke plumes, *J. Atmos. Chem.*, 55, 273-297, doi:10.1007/s10874-006-9039-5, 2006.

838

839 McDonald, J. D., Zielinska, B., Fujita, E. M., Sagebiel, J. C., Chow, J. C., and Watson, J. G.: Fine particle and
840 gaseous emission rates from residential wood combustion, *Environ. Sci. Technol.*, 34, 2080-2091,
841 doi:10.1021/es9909632, 2000.

842

843 McMeeking, G. R., Kreidenweis, S. M., Baker, S., Carrico, C. M., Chow, J. C., Collett, J. L., Hao, W. M.,
844 Holden, A. S., Kirchstetter, T. W., Malm, W. C., Moosmuller, H., Sullivan, A. P., and Wold, C. E.: Emissions
845 of trace gases and aerosols during the open combustion of biomass in the laboratory, *J. Geophys. Res.-*
846 *Atmos.*, 114, D19210, doi:10.1029/2009jd011836, 2009.

847

848 Murray, K. K., Boyd, R. K., Eberlin, M. N., Langley, G. J., Li, L., and Naito, Y.: Definitions of terms relating
849 to mass spectrometry (IUPAC Recommendations 2013), 85, 1515-1609, doi:10.1351/pac-rec-06-04-06,
850 2013.

851

852 Odum, J. R., Jungkamp, T. P. W., Griffin, R. J., Flagan, R. C., and Seinfeld, J. H.: The atmospheric aerosol-
853 forming potential of whole gasoline vapor, *Science*, 276, 96-99, 1997.

854

855 Pandis, S. N., Harley, R. A., Cass, G. R., and Seinfeld, J. H.: Secondary organic aerosol formation and
856 transport, *Atmos. Environ.*, 26, 2269-2282, 1992.

857

858 Roberts, J. M., Marchewka, M., Bertman, S. B., Sommariva, R., Warneke, C., de Gouw, J., Kuster, W.,
859 Goldan, P., Williams, E., Lerner, B. M., Murphy, P., and Fehsenfeld, F. C.: Measurements of PANs during
860 the New England air quality study 2002, *J. Geophys. Res.-Atmos.*, 112, D20306,
861 doi:10.1029/2007JD008667, 2007.

862

863 Roberts, J. M., Veres, P., Warneke, C., Neuman, J. A., Washenfelder, R. A., Brown, S. S., Baasandorj, M.,
864 Burkholder, J. B., Burling, I. R., Johnson, T. J., Yokelson, R. J., and de Gouw, J.: Measurement of HONO,
865 HNCO, and other inorganic acids by negative-ion proton-transfer chemical-ionization mass spectrometry
866 (NI-PT-CIMS): application to biomass burning emissions, *Atmos. Meas. Technol.*, 3, 981-990,
867 doi:doi:10.5194/amt-3-981-2010, 2010.

868

869 Roberts, J. M., Veres, P. R., Cochran, A. K., Warneke, C., Burling, I. R., Yokelson, R. J., Lerner, B., Gilman, J.
870 B., Kuster, W. C., Fall, R., and de Gouw, J.: Isocyanic acid in the atmosphere and its possible link to
871 smoke-related health effects, *Proc. Natl. Acad. Sci. U.S.A.*, 108, 8966-8971,
872 doi:10.1073/pnas.1103352108, 2011.

873
874 Schauer, J. J., Kleeman, M. J., Cass, G. R., and Simoneit, B. R. T.: Measurement of emissions from air
875 pollution sources. 3. C-1-C-29 organic compounds from fireplace combustion of wood, *Environ. Sci.*
876 *Technol.*, 35, 1716-1728, doi:10.1021/es001331e, 2001.

877
878 Simpson, I. J., Akagi, S. K., Barletta, B., Blake, N. J., Choi, Y., Diskin, G. S., Fried, A., Fuelberg, H. E.,
879 Meinardi, S., Rowland, F. S., Vay, S. A., Weinheimer, A. J., Wennberg, P. O., Wiebring, P., Wisthaler, A.,
880 Yang, M., Yokelson, R. J., and Blake, D. R.: Boreal forest fire emissions in fresh Canadian smoke plumes:
881 C₁-C₁₀ volatile organic compounds (VOCs), CO₂, CO, NO₂, NO, HCN and CH₃CN, *Atmos. Chem. Phys.*, 11,
882 6445-6463, doi:10.5194/acp-11-6445-2011, 2011.

883
884 Sommers, W. T., Loehman, R. A., and Hardy, C. C.: Wildland fire emissions, carbon, and climate: Science
885 overview and knowledge needs, *Forest Ecol. Manag.*, 317, 1-8, doi:10.1016/j.foreco.2013.12.014, 2014.

886
887 Stockwell, C. E., Yokelson, R. J., Kreidenweis, S. M., Robinson, A. L., DeMott, P. J., Sullivan, R. C., Reardon,
888 J., Ryan, K. C., Griffith, D. W. T., and Stevens, L.: Trace gas emissions from combustion of peat, crop
889 residue, domestic biofuels, grasses, and other fuels: configuration and Fourier transform infrared (FTIR)
890 component of the fourth Fire Lab at Missoula Experiment (FLAME-4), *Atmos. Chem. Phys.*, 14, 9727-
891 9754, doi:10.5194/acp-14-9727-2014, 2014.

892
893 Stockwell, C. E., Veres, P. R., Williams, J., and Yokelson, R. J.: Characterization of biomass burning
894 emissions from cooking fires, peat, crop residue, and other fuels with high-resolution proton-transfer-
895 reaction time-of-flight mass spectrometry, *Atmos. Chem. Phys.*, 15, 845-865, doi:10.5194/acp-15-845-
896 2015, 2015.

897
898 Trentmann, J., Andreae, M. O., and Graf, H. F.: Chemical processes in a young biomass-burning plume, *J.*
899 *Geophys. Res.-Atmos.*, 108, 4705-4714, doi:10.1029/2003jd003732, 2003.

900
901 Trentmann, J., Yokelson, R. J., Hobbs, P. V., Winterrath, T., Christian, T. J., Andreae, M. O., and Mason, S.
902 A.: An analysis of the chemical processes in the smoke plume from a savanna fire, *J. Geophys. Res.-*
903 *Atmos.*, 110, D12301, doi:10.1029/2004jd005628, 2005.

904
905 Tuazon, E. C., Alvarado, A., Aschmann, S. M., Atkinson, R., and Arey, J.: Products of the gas-phase
906 reactions of 1,3-butadiene with OH and NO₃ Radicals, *Environ. Sci. Technol.*, 33, 3586-3595,
907 doi:10.1021/es990193u, 1999.

908
909 Urbanski, S.: Wildland fire emissions, carbon, and climate: Emission factors, *Forest. Ecol. Manag.*, 317,
910 51-60, doi:10.1016/j.foreco.2013.05.045, 2014.

911
912 Veres, P., Roberts, J. M., Burling, I. R., Warneke, C., de Gouw, J., and Yokelson, R. J.: Measurements of
913 gas-phase inorganic and organic acids from biomass fires by negative-ion proton-transfer chemical-
914 ionization mass spectrometry, *J. Geophys. Res.-Atmos.*, 115, D23302, doi:10.1029/2010jd014033, 2010.

915

916 Warneke, C., Roberts, J. M., Veres, P., Gilman, J., Kuster, W. C., Burling, I., Yokelson, R., and de Gouw, J.
917 A.: VOC identification and inter-comparison from laboratory biomass burning using PTR-MS and PIT-MS,
918 Int. J. Mass Spectrom., 303, 6-14, doi:10.1016/j.ijms.2010.12.002, 2011.

919

920 Yokelson, R. J., Griffith, D. W. T., and Ward, D. E.: Open-path Fourier transform infrared studies of large-
921 scale laboratory biomass fires, J. Geophys. Res.-Atmos., 101, 21067-21080, 1996.

922

923 Yokelson, R. J., Burling, I. R., Gilman, J. B., Warneke, C., Stockwell, C. E., de Gouw, J., Akagi, S. K.,
924 Urbanski, S. P., Veres, P., Roberts, J. M., Kuster, W. C., Reardon, J., Griffith, D. W. T., Johnson, T. J.,
925 Hosseini, S., Miller, J. W., Cocker, D. R., Jung, H., and Weise, D. R.: Coupling field and laboratory
926 measurements to estimate the emission factors of identified and unidentified trace gases for prescribed
927 fires, Atmos. Chem. Phys., 13, 89-116, doi:10.5194/acp-13-89-2013, 2013.

928

929

930

931 **Table 1.** Measurement descriptions.
932
933

Instrument Identifier	Measurement Technique	Measurement Descriptions	Detection Qualifications	Instru. Details and Companion Papers
GC-MS	Gas chromatography-(Quadrupole) Mass Spectrometry	Discrete sampling via cryogenic pre-concentration, chromatographic separation, detection and identification via electron impact (EI) mass spectrum	Melting point greater than -185 °C; Boiling point less than 220 °C; Sufficiently non-polar (e.g., no acids); Fragment ion (m/z): 26 to 150	Goldan et al. (2004) Gilman et al. (2010) Yokelson et al. (2013)
PTR-MS	Proton Transfer Reaction-(Quadrupole) Mass Spectrometry	Real-time sampling via proton transfer reactions with H_3O^+ , quantification via protonated molecule $[\text{M}+\text{H}]^+$	Proton affinity greater than water; Protonated molecular mass (m/z): 20-240	Warneke et al. (2011) Yokelson et al. (2013)
PIT-MS	Proton Transfer Reaction-(Ion Trap) Mass Spectrometry	Real-time sampling via proton transfer reactions with H_3O^+ , quantification via protonated molecule $[\text{M}+\text{H}]^+$	Proton affinity greater than water; Protonated molecular mass (m/z): 20-240	Warneke et al. (2011) Yokelson et al. (2013)
NI-PT-CIMS	Negative Ion-Proton Transfer Reaction-(Quadrupole) Mass Spectrometry	Real-time sampling via proton transfer reactions with $\text{CH}_3\text{C}(\text{O})\text{O}^-$, quantification via deprotonated ion $[\text{M}-\text{H}]^-$	Gas-phase acidity greater than that of acetic acid; Deprotonated molecular mass (m/z): 10-225	Veres et al. (2011) Roberts et al. (2011) Yokelson et al. (2013)
OP-FTIR	Open Path-Fourier Transform Infrared Spectroscopy	Real-time spectral scanning via open path White cell (58 m pathlength), offline identification via compound specific infrared absorption features	Strong absorption features between 600-3400 cm^{-1} that are unique and free of interferences from other strong IR-absorbers (e.g., H_2O)	Burling et al. (2011) Yokelson et al. (2013)

934

935 **Table 2.** Mean VOC to CO discrete emission ratios (ERs, ppbv per ppmv CO) for the southwestern (SW), southeastern (SE), and northern (N)
 936 fuel regions.

Name	Formula	MW	D	m/z	SW Avg ER (± s.d.) npnts	SE Avg ER (± s.d.) npnts	N Avg ER (± s.d.) npnts	kOH	SOAP
Alkanes (Saturated, D = 0)									
Ethane	C2H6	30	0	27	1.8388 (1.2846)	25	4.5311 (3.8024)	23	6.8510 (3.5152)
Propane	C3H8	44	0	27	0.6317 (0.9985)	23	1.5957 (1.2193)	18	1.4633 (0.9354)
Butane_iso	C4H10	58	0	43	0.0522 (0.0813)	29	0.2984 (0.4734)	20	0.0982 (0.0620)
Butane_n	C4H10	58	0	43	0.1038 (0.1829)	29	0.3333 (0.2902)	20	0.4005 (0.2804)
Propane_22dimethyl*	C5H12	72	0	57	0.0003 (0.0008)	29	0.0004 (0.0008)	23	0.0006 (0.0007)
Pentane_iso	C5H12	72	0	43	0.0167 (0.0585)	29	0.0580 (0.0878)	23	0.0322 (0.0261)
Pentane_n	C5H12	72	0	43	0.0271 (0.0427)	29	0.0889 (0.0789)	23	0.1400 (0.1130)
Butane_22dimethyl	C6H14	86	0	71	0.0002 (0.0008)	29	0.0001 (0.0002)	23	0 (0.0002)
Pentane_3methyl	C6H14	86	0	57	0.0009 (0.0010)	9	0.0089 (0.0117)	16	0.0045 (0.0031)
Hexane_n	C6H14	86	0	57	0.0159 (0.0225)	29	0.0572 (0.0516)	23	0.0814 (0.0634)
Heptane_n	C7H16	100	0	43	0.0218 (0.0176)	9	0.0640 (0.0387)	14	0.0836 (0.0674)
Octane_n	C8H18	114	0	43	0.0138 (0.0128)	9	0.0469 (0.0281)	14	0.0536 (0.0353)
Nonane_n	C9H20	128	0	57	0.0085 (0.0079)	9	0.0358 (0.0213)	13	0.0369 (0.0269)
Decane_n	C10H22	142	0	57	0.0083 (0.0060)	9	0.0310 (0.0222)	14	0.0330 (0.0212)
Undecane_n	C11H24	156	0	57	0.0111 (0.0054)	8	0.0412 (0.0304)	12	0.0425 (0.0208)
Alkenes (Unsaturated, D = 1)									
Ethene	C2H4	28	1	27	5.8525 (4.1077)	25	8.1879 (4.2382)	21	18.3160 (12.8430)
Propene	C3H6	42	1	41	2.0801 (2.0528)	29	3.4917 (2.1610)	23	8.5115 (3.4340)
Propene_2methyl	C4H8	56	1	41	0.1046 (0.1652)	29	0.2668 (0.2151)	23	0.3162 (0.3624)
Butene_1	C4H8	56	1	41	0.2961 (0.3761)	29	0.4851 (0.3320)	23	1.5227 (0.6632)
Butene_cis2	C4H8	56	1	41	0.0579 (0.0937)	29	0.1209 (0.0920)	23	0.2397 (0.1916)
Butene_trans2	C4H8	56	1	41	0.0615 (0.1036)	29	0.1427 (0.1174)	23	0.2732 (0.2648)
Butene_1_2methyl	C5H10	70	1	55	0.0202 (0.0256)	29	0.0391 (0.0284)	23	0.0881 (0.0462)
Butene_1_3methyl	C5H10	70	1	55	0.0091 (0.0202)	8	0.0152 (0.0168)	15	0.0183 (0.0164)
Butene_2_2methyl	C5H10	70	1	55	0.0224 (0.0317)	8	0.0996 (0.0634)	14	0.1881 (0.0965)
Cyclopentane	C5H10	70	1	42	0.0024 (0.0040)	29	0.0064 (0.0053)	23	0.0108 (0.0074)
Pentene_1	C5H10	70	1	55	0.0429 (0.0654)	29	0.0902 (0.0773)	23	0.2311 (0.1872)
Pentene_cis2	C5H10	70	1	55	0.0432 (0.0638)	8	0.1396 (0.0883)	14	0.2905 (0.1492)
Pentene_trans2	C5H10	70	1	55	0.0276 (0.0341)	29	0.0422 (0.0304)	23	0.1180 (0.0667)
Cyclopentane_1methyl	C6H12	84	1	56	0.0040 (0.0037)	9	0.0147 (0.0139)	16	0.0159 (0.0113)
Pentene_1_2methyl*	C6H12	84	1	56	0.0890 (0.1102)	9	0.1782 (0.1162)	14	0.4980 (0.2945)

Cyclohexane	C6H12	84	1	84	0.0012	(0.0014)	9	0.0052	(0.0028)	14	0.0052	(0.0035)	4	7	0
Hexene_1	C6H12	84	1	84	0.1029	(0.1182)	8	0.2039	(0.0943)	12	0.4904	(0.2844)	4	37	0
Hexene_cis2	C6H12	84	1	84	0.0256	(0.0338)	9	0.0522	(0.0443)	16	0.1552	(0.0586)	4	62	1.3
Hexenes (Sum of 3 isomers)*	C6H12	84	1	84	0.0931	(0.1166)	9	0.1788	(0.1376)	16	0.5432	(0.2920)	4	62	1.3*
Cyclohexane_methyl	C7H14	98	1	83	0.0023	(0.0023)	8	0.0097	(0.0063)	14	0.0111	(0.0071)	4	9.6	0*
Heptene_1*	C7H14	98	1	56	0.0547	(0.0595)	9	0.1168	(0.0721)	14	0.2868	(0.1559)	4	38	0*
Octene_1	C8H16	112	1	55	0.0431	(0.0486)	9	0.1013	(0.0482)	13	0.1651	(0.0926)	4	36	0*
Nonene_1*	C9H18	126	1	41	0.0097	(0.0122)	9	0.0196	(0.0153)	16	0.0474	(0.0326)	4	42	1.9*
Decene_1*	C10H20	140	1	56	0.0133	(0.0159)	9	0.0260	(0.0228)	16	0.0812	(0.0415)	4	46	7*
Undecene_1*	C11H22	154	1	55	0.0103	(0.0100)	9	0.0279	(0.0292)	16	0.0647	(0.0251)	4	48	16*

Alkynes and Alkenes (Polyunsaturated, D > 1)

Ethyne	C2H2	26	2	IR	2.3905	(3.0119)	27	1.7412	(1.3580)	23	5.0910	(5.6894)	4	0.9	0.1
Propyne*	C3H4	40	2	39	0.2093	(0.1503)	29	0.1850	(0.1626)	23	0.7876	(0.6405)	4	3.1	0*
Butadiyne_13 (Diacetylene)*	C4H2	50	4	50	0.0080	(0.0054)	9	0.0041	(0.0052)	16	0.0427	(0.0651)	4	16	0*
Butenyne (Vinylacetylene)*	C4H4	52	3	52	0.0285	(0.0452)	9	0.0154	(0.0190)	16	0.0824	(0.1062)	4	20*	0*
Butadiene_12*	C4H6	54	2	54	0.0101	(0.0146)	29	0.0087	(0.0095)	23	0.0441	(0.0343)	4	27	1.8*
Butadiene_13	C4H6	54	2	54	0.4065	(0.5315)	29	0.4122	(0.3530)	23	1.8781	(0.9509)	4	67	1.8
Butyne (1- or 2-)*	C4H6	54	2	54	0.0221	(0.0287)	9	0.0158	(0.0146)	16	0.0693	(0.0300)	4	8*	0*
Cyclopentadiene_13*	C5H6	66	3	66	0.1724	(0.3868)	8	0.1747	(0.0992)	14	0.5836	(0.3458)	4	92	0*
Pentenyne isomer (e.g., propenylacetylene)*	C5H6	66	3	66	0.0161	(0.0176)	9	0.0107	(0.0119)	16	0.0651	(0.0395)	4	92*	0*
Butyne_3methyl*	C5H8	68	2	67	0.0090	(0.0166)	9	0.0103	(0.0108)	16	0.0426	(0.0303)	4	11*	0*
Cyclopentene*	C5H8	68	2	67	0.0699	(0.1240)	7	0.1125	(0.0789)	14	0.2815	(0.1725)	4	57	1.8*
Pentadiene_cis13	C5H8	68	2	67	0.0457	(0.0795)	8	0.0627	(0.0360)	14	0.1733	(0.0691)	4	83	1.8*
Pentadiene_trans13	C5H8	68	2	67	0.0668	(0.1069)	9	0.1044	(0.0538)	14	0.2504	(0.0927)	4	83	1.8*
Hexadienyne (e.g., divinylacetylene)*	C6H6	78	4	78	0.0140	(0.0152)	9	0.0088	(0.0072)	16	0.0569	(0.0382)	4	67*	1.8*
Cyclopentadiene_methyl (Sum of 2 isomers)*	C6H8	80	3	79	0.0242	(0.0329)	9	0.0516	(0.0554)	16	0.1831	(0.1771)	4	103*	1.8*
Hexenyne (e.g., 2-methyl-1-penten-3-yne)*	C6H8	80	3	80	0.0110	(0.0127)	9	0.0102	(0.0117)	16	0.0674	(0.0545)	4	37*	1*
Cyclohexene	C6H10	82	2	67	0.0170	(0.0235)	9	0.0345	(0.0205)	14	0.0927	(0.0506)	4	62	0*
Cyclopentene_1methyl*	C6H10	82	2	67	0.0202	(0.0298)	9	0.0466	(0.0259)	13	0.1109	(0.0539)	4	60*	0*
Hexadiene_cis13*	C6H10	82	2	67	0.0026	(0.0037)	9	0.0044	(0.0030)	14	0.0097	(0.0018)	4	97	1.8*
Hexadiene_trans13*	C6H10	82	2	67	0.0039	(0.0081)	9	0.0045	(0.0042)	12	0.0266	(0.0151)	4	97	1.8*
Other C6H10 (Sum of 5 isomers)*	C6H10	82	2	67	0.0348	(0.0466)	9	0.0531	(0.0418)	16	0.1954	(0.0798)	4	97*	1*

Heptadiyne (Sum of 2 isomers)*	C7H8	92	4	91	0.0073	(0.0094)	9	0.0035	(0.0053)	16	0.0464	(0.0394)	4	2*	1*
Cyclohexene_1methyl*	C7H12	96	2	81	0.0098	(0.0120)	8	0.0262	(0.0139)	13	0.0437	(0.0259)	4	96	0*
Octadiene*	C8H14	110	2	55	0.0347	(0.0531)	9	0.0673	(0.0416)	16	0.1387	(0.0536)	4	110	1.9*
Nonadiene*	C9H16	124	2	54	0.0020	(0.0027)	9	0.0048	(0.0048)	16	0.0171	(0.0077)	4	120*	1.9*
C10H14 non-aromatic (e.g., hexahydronaphthalene)*	C10H14	134	4	91	0.0013	(0.0018)	9	0.0041	(0.0055)	16	0.0155	(0.0090)	4	130*	90*
Terpenes (Polyunsaturated, D > 1)															
Isoprene	C5H8	68	2	67	0.1289	(0.1447)	29	0.2428	(0.1944)	23	0.6942	(0.4405)	4	100	1.9
Camphepane	C10H16	136	3	93	0.0032	(0.0026)	9	0.0538	(0.0979)	14	0.1193	(0.1459)	4	53	18*
Carene_3	C10H16	136	3	93	0.0050	(0.0052)	8	0.0289	(0.0303)	12	0.1578	(0.2107)	4	85	18*
Limonene_D	C10H16	136	3	68	0.0219	(0.0249)	29	0.1232	(0.1302)	23	0.8384	(1.1869)	4	170	18*
Limonene_iso*	C10H16	136	3	68	0.0002	(0.0005)	9	0.0094	(0.0109)	16	0.0237	(0.0206)	4	170	18*
Myrcene*	C10H16	136	3	93	0.0075	(0.0106)	8	0.0068	(0.0055)	10	0.1313	(0.1849)	4	200	18
Pinene_alpha	C10H16	136	3	93	0.0058	(0.0051)	9	0.1013	(0.1454)	15	0.8105	(1.2079)	4	52	17
Pinene_beta	C10H16	136	3	93	0.0051	(0.0092)	29	0.0194	(0.0220)	23	0.1638	(0.1545)	4	74	18*
Terpinene_gamma*	C10H16	136	3	93	0.0044	(0.0026)	5	0.0118	(0.0066)	4	0.0310	(0.0336)	2	177	18*
Terpinolene*	C10H16	136	3	93	0.0053	(0.0020)	4	0.0131	(0.0163)	8	0.0339	(0.0435)	4	225	18*
Sesquiterpenes (Sum of all isomers)	C15H24	204	4	205+	0.0092	(0.0088)	29	0.0669	(0.0786)	23	0.0915	(0.0659)	4	300*	20*
Aromatics with saturated substituents (D = 4)															
Benzene	C6H6	78	4	78	0.8385	(0.7301)	29	0.7008	(0.3680)	23	2.1381	(1.3236)	4	1.2	93
Toluene	C7H8	92	4	91	0.3549	(0.3417)	29	0.6196	(0.4414)	23	1.3375	(0.5725)	4	5.6	100
Benzene_ethyl	C8H10	106	4	91	0.0495	(0.0498)	29	0.0829	(0.0583)	23	0.1766	(0.0919)	4	7.5	112
Xylene_o	C8H10	106	4	91	0.0391	(0.0418)	29	0.0730	(0.0527)	23	0.1429	(0.0579)	4	14	96
Xylenes_m&p (Sum of 2 isomers)	C8H10	106	4	91	0.0981	(0.1136)	29	0.2107	(0.1546)	23	0.5088	(0.2484)	4	19*	76*
Benzene_123trimethyl	C9H12	120	4	105	0.0150	(0.0137)	9	0.0617	(0.0425)	15	0.0906	(0.0562)	4	29	44
Benzene_124trimethyl	C9H12	120	4	105	0.0172	(0.0217)	29	0.0416	(0.0291)	23	0.0828	(0.0339)	4	32	21
Benzene_135trimethyl	C9H12	120	4	105	0.0090	(0.0083)	9	0.0234	(0.0154)	15	0.0401	(0.0158)	4	60	14
Benzene_1ethyl_2methyl	C9H12	120	4	105	0.0094	(0.0114)	9	0.0164	(0.0122)	15	0.0374	(0.0193)	4	13	95
Benzene_1ethyl_3&4_methyl (Sum of 2 isomers)	C9H12	120	4	105	0.0186	(0.0228)	29	0.0395	(0.0312)	23	0.1265	(0.0737)	4	16*	85*
Benzene_isoPropyl	C9H12	120	4	105	0.0041	(0.0042)	9	0.0073	(0.0065)	14	0.0290	(0.0211)	4	6.6	96
Benzene_nPropyl	C9H12	120	4	91	0.0081	(0.0096)	9	0.0173	(0.0102)	14	0.0331	(0.0204)	4	5.7	110
Benzene_isoButyl	C10H14	134	4	91	0.0056	(0.0065)	9	0.0119	(0.0104)	16	0.0248	(0.0145)	4	7*	90*
Benzene_nButyl	C10H14	134	4	91	0.0065	(0.0078)	9	0.0151	(0.0129)	16	0.0329	(0.0193)	4	7*	90*

Benzene_1methyl_4isopropyl (p-Cymene)	C10H14	134	4	119	0.1081	(0.2713)	29	0.1030	(0.0974)	23	0.1726	(0.1400)	4	15	95*
Benzene_nPropyl_methyl (Sum of 2 isomers)*	C10H14	134	4	105	0.0074	(0.0084)	9	0.0200	(0.0187)	16	0.0420	(0.0213)	4	10*	95*
Benzene_14diethyl	C10H14	134	4	119	0.0007	(0.0011)	9	0.0018	(0.0039)	16	0.0165	(0.0074)	4	10*	90*
Xylene_ethyl (Sum of 2 isomers)*	C10H14	134	4	119	0.0093	(0.0102)	9	0.0149	(0.0144)	16	0.0379	(0.0158)	4	10*	90*
Aromatics with unsaturated substituents (D > 4)															
Benzene_ethylvinyl (Phenylethyne)*	C8H6	102	6	102	0.0323	(0.0238)	9	0.0153	(0.0163)	16	0.0686	(0.0700)	4	1*	90*
Styrene (Phenylethene)	C8H8	104	5	104	0.0883	(0.0840)	29	0.1067	(0.1054)	23	0.3361	(0.2437)	4	43	212
Indene*	C9H8	116	6	115	0.0358	(0.0446)	9	0.0408	(0.0325)	16	0.1311	(0.1116)	4	51	90
Benzene_1propenyl*	C9H10	118	5	117	0.0046	(0.0054)	9	0.0039	(0.0045)	16	0.0135	(0.0074)	4	60	200*
Benzene_2propenyl*	C9H10	118	5	117	0.0067	(0.0066)	9	0.0097	(0.0080)	16	0.0236	(0.0103)	4	60	200*
Benzene_isopropenyl*	C9H10	118	5	118	0.0052	(0.0059)	9	0.0049	(0.0050)	16	0.0232	(0.0129)	4	53	200*
Styrene_2methyl*	C9H10	118	5	117	0.0142	(0.0125)	9	0.0153	(0.0140)	16	0.0414	(0.0176)	4	53*	200*
Styrene_3methyl*	C9H10	118	5	117	0.0229	(0.0255)	9	0.0297	(0.0234)	16	0.0865	(0.0420)	4	53*	200*
Styrene_4methyl*	C9H10	118	5	117	0.0080	(0.0097)	9	0.0143	(0.0116)	16	0.0314	(0.0122)	4	53*	200*
Indane*	C9H10	118	5	117	0.0084	(0.0066)	8	0.0155	(0.0069)	13	0.0261	(0.0108)	4	19	90
Naphthalene*	C10H8	128	7	128	0.0070	(0.0048)	9	0.0040	(0.0050)	16	0.0215	(0.0122)	4	23	200*
Indene_1or3methyl*	C10H10	130	6	130	0.0010	(0.0009)	9	0.0004	(0.0011)	16	0.0079	(0.0059)	4	51*	200*
Naphthalene_12dihydro*	C10H10	130	6	130	0.0062	(0.0054)	9	0.0099	(0.0103)	16	0.0277	(0.0106)	4	23*	90*
Naphthalene_13dihydro*	C10H10	130	6	130	0.0062	(0.0066)	9	0.0099	(0.0113)	16	0.0339	(0.0120)	4	23*	90*
Benzene_1butenyl*	C10H12	132	5	117	0.0021	(0.0028)	9	0.0027	(0.0038)	16	0.0140	(0.0048)	4	33*	200*
Benzene_methylpropenyl (2- phenyl-2-butene)*	C10H12	132	5	117	0.0274	(0.0443)	9	0.0179	(0.0179)	16	0.0436	(0.0270)	4	33	200*
Styrene_ethyl*	C10H12	132	5	117	0.0048	(0.0052)	9	0.0063	(0.0105)	16	0.0196	(0.0085)	4	33*	200*
Nitrogen-containing organics															
Acid_Hydrocyanic (Hydrogen cyanide)	HCN	27	2	IR	1.2331	(1.2922)	29	2.7807	(1.6904)	23	3.0223	(2.2719)	4	0.03	1*
Acid_Isocyanic	HNCO	43	2	42-	0.8433	(0.6858)	16	0.8046	(0.5742)	17	1.3360	(0.2301)	2	0	1*
Methylnitrite (Nitrous acid, methyl ester)*	CH3NO2	61	1	61	0.8994	(1.1114)	7	0.5241	(0.5064)	12	0.7641	(0.8964)	3	0.3	1*
Nitromethane*	CH3NO2	61	1	61	0.0272	(0.0237)	9	0.0323	(0.0326)	16	0.0713	(0.0868)	4	0.02	1*
Acetonitrile	C2H3N	41	2	41	0.7731	(0.9389)	29	0.9841	(0.5366)	23	1.6524	(0.8811)	4	0.02	1*
Hydrazine_11dimethyl*	C2H8N2	60	0	60	0.0636	(0.1324)	9	0.1360	(0.2705)	16	0.1976	(0.2297)	4	60	0*
Propenenitrile_2 (Acrylonitrile)	C3H3N	53	3	53	0.0869	(0.0731)	29	0.1199	(0.0754)	23	0.3217	(0.2551)	4	4.0	1*

Propanenitrile (Cyanoethane)*	C3H5N	55	2	54	0.0314	(0.0380)	9	0.0432	(0.0366)	16	0.0981	(0.0803)	4	0.26	1*
Pyrrole*	C4H5N	67	3	67	0.0393	(0.0591)	9	0.0367	(0.0392)	16	0.1066	(0.1088)	4	145	1*
Pyrazole_1methyl*	C4H6N2	82	3	82	0.0074	(0.0073)	9	0.0198	(0.0176)	16	0.0359	(0.0161)	4	150*	1*
Diazine_methyl (Sum of 3 isomers)*	C5H6N2	94	4	94	0.0292	(0.0312)	9	0.0535	(0.0456)	16	0.1125	(0.0303)	4	10*	1*
Pyrrole_1methyl*	C5H7N	81	3	80	0.0202	(0.0299)	9	0.0083	(0.0105)	16	0.0217	(0.0304)	4	145*	1*
Pyrazine_2ethyl*	C6H8N2	108	4	108	0.0062	(0.0092)	9	0.0152	(0.0113)	16	0.0296	(0.0168)	4	10*	1*
Benzonitrile (Cyanobenzene)	C7H5N	103	6	103	0.0622	(0.0334)	9	0.1395	(0.0757)	16	0.1380	(0.0746)	4	1*	90*
O VOCs with low degrees of unsaturation (D ≤ 1)															
Formaldehyde	CH2O	30	1	IR	5.3939	(3.1497)	29	12.2348	(7.2935)	23	17.9180	(10.5410)	4	9.4	0.7
Acid_Formic	CH2O2	46	1	IR	0.6359	(0.5705)	29	1.6007	(1.1054)	23	1.7538	(1.9738)	4	0.45	0.1
Methanol	CH4O	32	0	31	3.6175	(2.9726)	29	7.7807	(5.5412)	23	13.6981	(8.7348)	4	0.9	0.3
Acetaldehyde	C2H4O	44	1	44	1.5503	(1.1511)	29	2.8332	(1.8131)	23	5.4742	(3.5540)	4	16	0.6
Acid_Acetic	C2H4O2	60	1	IR	5.3926	(3.2343)	29	13.0293	(8.8369)	23	9.6068	(6.2350)	4	0.7	0.1
Formate_methyl (Formic Acid, methyl ester)	C2H4O2	60	1	60	0.0675	(0.0390)	8	0.1031	(0.0626)	15	0.2096	(0.0831)	4	0.18	0.1
Acid_Glycolic	C2H4O3	76	1	75-	0.0068	(0.0061)	15	0.1183	(0.1251)	17	0.0114	(0.0115)	2	0.50*	0.1*
Ethanol	C2H6O	46	0	31	0.0498	(0.0617)	29	0.4817	(0.8472)	23	0.2673	(0.1892)	4	3.4	0.6
Acetone	C3H6O	58	1	43	0.6501	(0.7408)	29	1.6035	(1.1498)	23	2.6208	(1.0656)	4	0.19	0.3
Propanal	C3H6O	58	1	58	0.2135	(0.2333)	29	0.4497	(0.3177)	23	0.9246	(0.3186)	4	20	0.5
Acetate_methyl (Acetic Acid, methyl ester)*	C3H6O2	74	1	74	0.4593	(0.4854)	9	0.6741	(0.4345)	16	0.6537	(0.3598)	4	0.35	0.1
Formate_ethyl (Formic Acid, ethyl ester)*	C3H6O2	74	1	30	0.0214	(0.0157)	5	0.0349	(0.0160)	10	0.0472	(0.0228)	4	0.96	0.1*
Butanal_n	C4H8O	72	1	72	0.0496	(0.0610)	29	0.0850	(0.0641)	23	0.1971	(0.0829)	4	24	0
Butanone_2 (MEK)	C4H8O	72	1	43	0.1788	(0.2216)	29	0.4143	(0.3061)	23	0.8027	(0.3109)	4	1.2	0.6
Propanal_2methyl*	C4H8O	72	1	72	0.0535	(0.0599)	9	0.1426	(0.0933)	15	0.1657	(0.0976)	4	27	0.3
Propanoate_methyl (Propanoic Acid, methyl ester)*	C4H8O2	88	1	88	0.0064	(0.0085)	9	0.0081	(0.0082)	16	0.0186	(0.0110)	4	0.88	0.1*
Butanol_1*	C4H10O	74	0	56	0.8294	(1.6678)	8	0.2327	(0.2540)	16	0.1434	(0.0695)	4	8.5	0.3
Butanal_2methyl*	C5H10O	86	1	57	0.0442	(0.0476)	9	0.1398	(0.0760)	13	0.1323	(0.0939)	4	31	0.3*
Butanone_2_3methyl*	C5H10O	86	1	43	0.0243	(0.0315)	9	0.0780	(0.0394)	14	0.1092	(0.0551)	4	3.0	0.3
Pentanone_2	C5H10O	86	1	43	0.0576	(0.0457)	8	0.1095	(0.0537)	14	0.1791	(0.0935)	4	4.6	0.6
Pentanone_3	C5H10O	86	1	57	0.0381	(0.0366)	8	0.0869	(0.0483)	15	0.1330	(0.0562)	4	2.9	0.4
Butanoate_methyl (Butyric Acid, methyl ester)*	C5H10O2	102	1	74	0.0024	(0.0041)	9	0.0558	(0.1431)	16	0.0097	(0.0063)	4	3.5	0.1*

Hexanal_n	C6H12O	100	1	56	0.0192	(0.0223)	29	0.0342	(0.0224)	23	0.0635	(0.0431)	4	28	0*
Hexanone_2	C6H12O	100	1	43	0.0101	(0.0063)	8	0.0269	(0.0092)	12	0.0462	(0.0268)	4	6.2	0.3
Hexanone_3	C6H12O	100	1	43	0.0314	(0.0315)	9	0.0834	(0.0317)	13	0.1646	(0.0868)	4	7.0	0
OVOCs with high degrees of unsaturation (D > 1)															
Propenal_2 (Acrolein)	C3H4O	56	2	56	0.8189	(0.6824)	29	1.3107	(0.8806)	23	3.5441	(1.6919)	4	20	1*
Acid_Acrylic	C3H4O2	72	2	71-	0.0409	(0.0438)	16	0.2159	(0.1637)	17	0.3672	(0.3881)	2	26*	1*
Acid_Pyruvic	C3H4O3	88	2	87-	0.0140	(0.0140)	15	0.1073	(0.1266)	17	0.0562	(0.0537)	2	0.12	0.1*
Butenal_2 (Crotonaldehyde)	C4H6O	70	2	70	0.1218	(0.1286)	29	0.3234	(0.2207)	23	0.5275	(0.1642)	4	35	1*
Methacrolein (MACR)	C4H6O	70	2	41	0.0895	(0.1077)	29	0.1807	(0.1257)	23	0.5501	(0.3146)	4	31	1*
Methylvinylketone (MVK)	C4H6O	70	2	55	0.4003	(0.5191)	29	0.8953	(0.6389)	23	2.1216	(0.8712)	4	19	1*
Butadione_23	C4H6O2	86	2	86	0.2147	(0.2059)	29	0.6435	(0.4616)	23	1.2062	(0.5357)	4	0.25	0.3*
Acrylate_methyl (2-Propenoic Acid, methyl ester)	C4H6O2	86	2	85	0.0159	(0.0178)	9	0.0223	(0.0149)	16	0.0470	(0.0227)	4	13	1*
Acetate_vinyl (Acetic Acid, vinyl ester)	C4H6O2	86	2	86	0.0004	(0.0012)	9	0.0000	0.0000	16	0.0048	(0.0095)	4	25	1*
Dioxin_14_23dihydro*	C4H6O2	86	2	58	0.0023	(0.0044)	9	0.0043	(0.0059)	16	0.0179	(0.0162)	4	20*	0.1*
Cyclopentenedione*	C5H4O2	96	4	96	0.0056	(0.0080)	9	0.0265	(0.0337)	16	0.0401	(0.0326)	4	57*	1*
Cyclopentenone*	C5H6O	82	3	82	0.0825	(0.1208)	9	0.9873	(1.1659)	16	0.9221	(0.6570)	4	57*	1*
Pentenone (e.g., Ethyl vinyl ketone)*	C5H8O	84	2	84	0.2682	(0.4437)	9	0.8946	(0.5222)	16	1.4135	(0.6686)	4	36*	1*
Pantanone_cyclo	C5H8O	84	2	84	0.1145	(0.1015)	9	0.3433	(0.2471)	16	0.7012	(0.2870)	4	2.9	1*
Butenal_2_methyl	C5H8O	84	2	84	0.0072	(0.0064)	9	0.0250	(0.0210)	16	0.0384	(0.0136)	4	52	1*
Methacrylate_methyl (Methacrylic acid, methyl ester)	C5H8O2	100	2	100	0.0306	(0.0333)	9	0.1055	(0.0335)	13	0.1287	(0.0537)	4	43	1*
Phenol	C6H6O	94	4	95+	0.4262	(0.4242)	25	0.7740	(0.6275)	21	2.4947	(1.6182)	4	28	<u>150*</u>
Benzene_12&13diol (Sum of 2 isomers)	C6H6O2	110	4	109-	0.2438	(0.1859)	13	3.1107	(3.3461)	17	3.9631	(1.9126)	2	5.0*	<u>200*</u>
Benzaldehyde	C7H6O	106	5	77	0.2212	(0.1661)	29	0.4717	(0.3259)	23	0.6995	(0.2661)	4	13	216
Phenol_methyl (Sum of cresol isomers)	C7H8O	108	4	109+	0.4807	(0.4799)	25	0.7770	(0.6290)	21	2.0703	(1.4093)	4	45*	<u>150*</u>
Furans (heterocyclic OVOCs, D ≥ 1)															
Furan	C4H4O	68	3	68	0.2680	(0.2474)	29	0.7302	(0.4732)	23	1.1090	(0.4337)	4	40	1*
Furan_25dihydro*	C4H6O	70	2	70	0.0083	(0.0126)	9	0.0154	(0.0438)	16	0.0071	(0.0141)	4	25*	1*
Furan_tetrahydro*	C4H8O	72	1	72	0.0022	(0.0027)	9	0.0014	(0.0027)	16	0.0101	(0.0067)	4	15	1*
Furaldehyde_2 (Furfural)	C5H4O2	96	4	95	0.3567	(0.2119)	9	1.5298	(1.0837)	16	1.2999	(0.6550)	4	35	1*
Furaldehyde_3*	C5H4O2	96	4	95	0.0152	(0.0135)	9	0.0585	(0.0403)	16	0.0687	(0.0330)	4	49	1*
Furan_2methyl	C5H6O	82	3	82	0.2847	(0.3634)	9	0.6908	(0.4118)	16	1.2105	(0.4806)	4	62	1*
Furan_3methyl	C5H6O	82	3	82	0.0272	(0.0311)	29	0.0776	(0.0582)	23	0.1758	(0.0661)	4	94	1*
Furan_25dimethyl*	C6H8O	96	3	96	0.0328	(0.0472)	9	0.0857	(0.0587)	16	0.1808	(0.1005)	4	132	1*

Furan_2ethyl	C6H8O	96	3	81	0.0167	(0.0218)	29	0.0387	(0.0285)	23	0.0821	(0.0288)	4	108	1*
Benzofuran	C8H6O	118	6	118	0.0902	(0.0666)	9	0.1366	(0.0734)	16	0.2504	(0.0957)	4	37	90*
Benzofuran_methyl (Sum of 4 isomers)*	C9H8O	132	6	131	0.0599	(0.0444)	9	0.1078	(0.0938)	16	0.1980	(0.0363)	4	37*	90*
Methane and Inorganic Gases															
Methane	CH4	16	—	IR	40.911	(24.945)	29	62.302	(32.218)	23	96.707	(28.737)	4	0.006	0
Carbon Monoxide	CO	28	—	IR	1000	(0)	29	1000	(0)	23	1000	(0)	4	0.15	0
Carbon Dioxide	CO2	44	—	IR	18202	(20970)	29	31170	(71256)	23	17999	(14000)	4	0	0
Tricarbon Dioxide (Carbon suboxide)	C3O2	68	—	68	0.0024	(0.0030)	9	0.0040	(0.0055)	16	0.0044	(0.0042)	4	1.5	0
Ammonia	NH3	17	—	IR	12.530	(8.838)	29	14.797	(6.131)	23	20.761	(16.928)	4	0.15	0
Nitrogen Oxide	NO	30	—	IR	38.788	(51.194)	29	39.695	(91.842)	23	26.530	(24.243)	4	0	0
Nitrogen Dioxide	NO2	46	—	IR	7.051	(8.565)	29	12.254	(21.246)	23	10.583	(10.218)	4	8.7	0
Nitrous Acid	HONO	47	—	46-	2.504	(2.827)	16	4.563	(6.049)	17	4.946	(5.254)	2	6.0	0
Sulfur Dioxide	SO2	64	—	IR	5.600	(9.993)	29	7.901	(14.488)	23	8.408	(5.347)	4	2.0	0
Hydrochloric Acid	HCl	36	—	IR	0.992	(2.574)	29	1.398	(4.825)	23	0.472	(0.719)	4	0.08	0
Total ERs (mmol/mol CO):				19356			32403			19317					
\sum ERs for all nitrogen-containing species:				65	0.34%	N	77	0.24%	N	71	0.37%	N			
\sum ERs for all VOCs and % of total emissions:				46	0.24%	VOC	90	0.28%	VOC	150	0.78%	VOC			
\sum ERs for unsaturated VOCs and % of total VOC:				39	84%	Unsat	74	82%	Unsat	126	84%	Unsat			
\sum ERs for oxygenated VOCs and % of total VOC:				24	53%	Oxy	57	63%	Oxy	81	54%	Oxy			

937

938 **Table 2 footnotes:**

939 Description of naming scheme: propane_22dimethyl is equivalent to 2,2-dimethylpropane. If the exact compound identity could not be determined, then the
 940 species are identified using general names that reflect the chemical family and formula are used. For example, hexenes (sum of 3 isomers) may include
 941 species such as cis- and trans-3-hexene. Alternative names, such as p-Cymene for 1-methyl-4-isopropylbenzene, or common abbreviations such as MEK
 942 for Butanone_2 are also included. (*) Identifies species whose calibration factors were estimated.

943 MW = molecular weight (g/mol); D = degree of unsaturation; *m/z* = fragment ion used to quantify a species by GC-MS where (+) denotes the protonated mass
 944 measured by PTR-MS or PIT-MS, (-) denotes the deprotonated mass measured by NI-PT-CIMS, and (IR) denotes measurements by OP-FTIR.

945 ER = emission ratio in units of ppbv per ppmv CO equivalent to mmol per mol CO

946 avg = mean; s.d. = standard deviation; and npnts = number of points used to calculate average and standard deviation.

947 **Bold ER** = Largest 3 ERs for each compound class;

948 **Bold and Italicized ER** = Largest 3 ERs for all VOCs

949 kOH = second-order reaction rate coefficients of VOC + OH reaction at STP ($\times 10^{12}$ cm 3 molec $^{-1}$ s $^{-1}$) from the National Institute of Standards and Technology's
 950 Chemical Kinetics Database and the references therein (Manion et al., 2015). (*) Identifies estimated kOH values.

951 SOAP = "secondary organic aerosol potential" values from Derwent et al. (2010). (*) Identifies estimated SOAP values.

952 **Bold kOH or SOAP values** = The largest 3 contributors to either OH reactivity or SOAP values for each compound class

953 **Bold and italicized kOH or SOAP values** = The largest 3 contributors to either OH reactivity or SOAP values for all VOCs

954 **Table 3.** Slopes and correlation coefficients (r) for VOC to carbon monoxide (CO) and VOC to acetonitrile (CH_3CN) ratios observed in biomass
 955 burning (BB) plumes from the Fourmile Canyon Fire as identified in Figure .

Name	VOC vs. CO		VOC vs. CH_3CN		Emission sources			Rxn Rate Coef.	
	Slope	r	Slope	r	BB	Urban	Biogenic	kOH	vs. CH_3CN
Carene_3	0.420	0.96	0.065	0.97	yes		yes	85	4250
Butadiene_13	0.193	0.98	0.030	0.94	yes	yes		67	3330
Furan_2methyl	0.285	0.88	0.047	0.95	yes			62	3100
Propene_2methyl	0.422	0.98	0.065	0.98	yes	yes		51	2570
Styrene	0.140	0.97	0.021	0.94	yes	yes	yes	43	2150
Furan	0.513	0.70	0.115	0.95	yes			40	2000
Benzofuran	0.132	0.97	0.021	0.99	yes			37	1860
Furaldehyde_2	0.304	0.93	0.049	0.98	yes			35	1750
Butene_1	0.367	0.98	0.057	0.99	yes	yes		31	1570
Propene	4.161	0.97	0.639	0.99	yes	yes		26	1315
Propenal_2	0.894	0.98	0.137	0.98	yes	yes		20	1000
Propanal	1.063	0.95	0.148	0.90	yes	yes		20	1000
p-Cymene*	0.268	0.97	0.041	0.97	yes		yes	15	750
Benzaldehyde	0.979	0.98	0.144	0.95	yes		yes	13	650
Ethene	8.635	0.97	1.353	0.92	yes	yes		8.5	425
Benzene	1.894	0.99	0.284	0.96	yes	yes		1.2	60
Butanone_2 (MEK)	1.129	0.93	0.164	0.94	yes	yes	yes	1.2	60
Benzonitrile	0.308	0.88	0.050	0.94	yes			1.0	50
Butadione_23	0.224	0.77	0.038	0.88	yes		yes	0.25	13
Acetonitrile	6.724	0.96	1.000	1.00	yes			0.02	1

956

957 **Table 3 footnotes:**

958 VOC to CO slope is in units of (ppbv VOC per ppmv CO)

959 VOC to CH_3CN slope is in units of (ppbv VOC per ppbv CH_3CN)

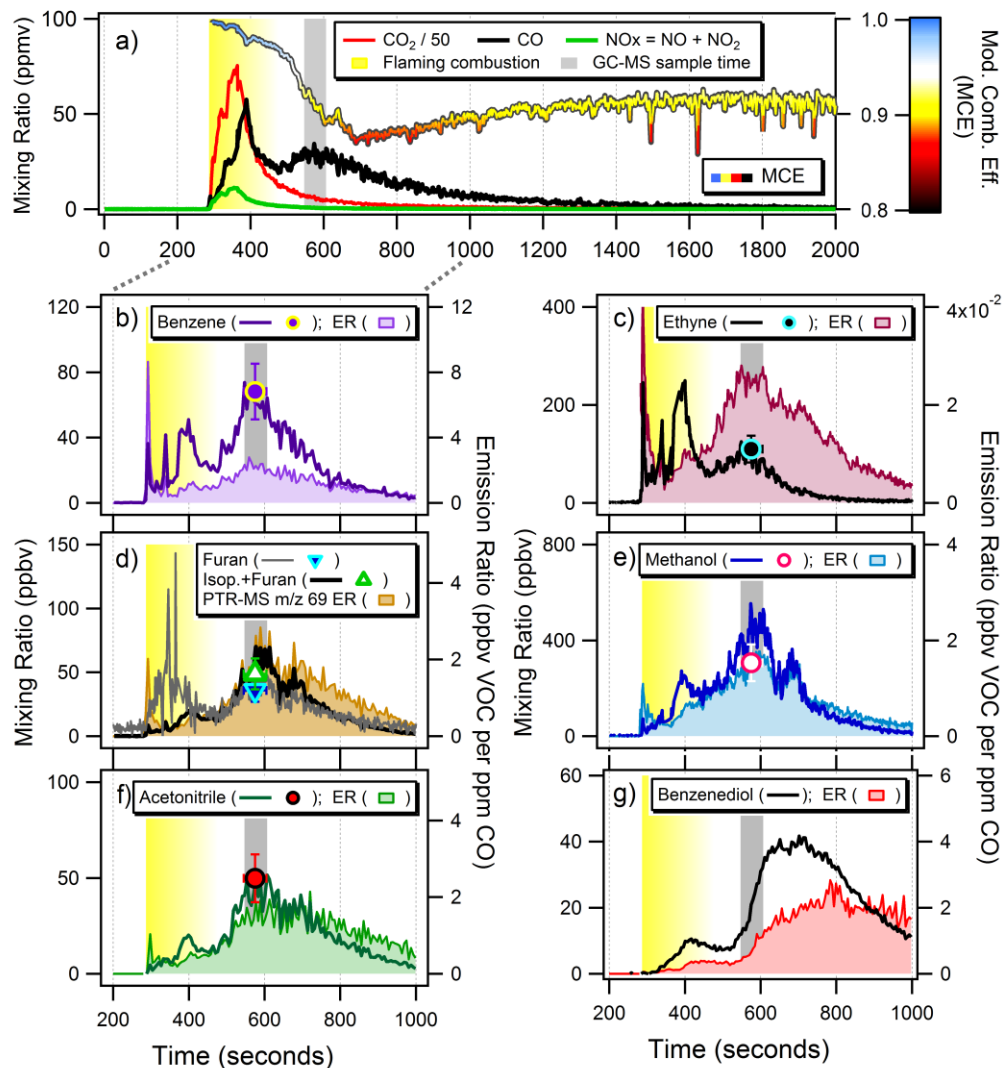
960 **Bold** face denotes VOCs that are the best available BB markers.

961 * kOH = second-order reaction rate coefficients of VOC + OH reaction at STP ($\times 10^{12} \text{ cm}^3 \text{ molec}^{-1} \text{ s}^{-1}$) from the National Institute of Standards and
 962 Technology's Chemical Kinetics Database and the references therein (Manion et al., 2015).

963 ** Ratio of $k\text{OH}_{\text{VOC}}/k\text{OH}_{\text{CH}_3\text{CN}}$ at STP

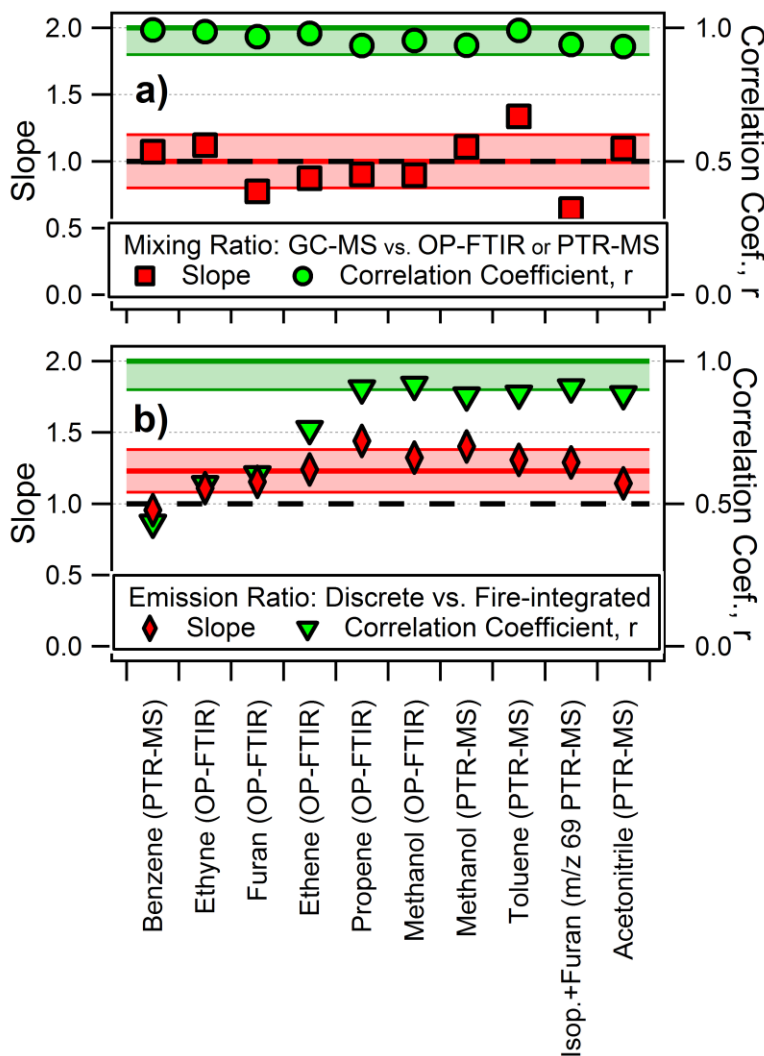
964 ***Benzene_1methyl_4isopropyl

965 **Figure 1.** Temporal profiles of mixing ratios and emission ratios (ER) of selected gases and the modified
 966 combustion efficiency (MCE) for an example laboratory burn of Emory Oak Woodland fuel from Fort
 967 Huachuca, Arizona. a) Mixing ratios of CO_2 , CO, and NOx measured by OP-FTIR. The MCE trace is
 968 colored by the key and scale on the right. The vertical bars represent the flaming combustion phase of
 969 the laboratory burn (yellow) and the GC-MS sample acquisition time (grey). b-f) Discrete GC-MS
 970 measured mixing ratios are shown as markers. b-g) Mixing ratios measured by PTR-MS (benzene, m/z
 971 69 = isoprene+furan+other, and acetonitrile), OP-FTIR (furan, ethyne, and methanol), and NI-PT-CIMS
 972 (benzenediol) are shown as lines and the corresponding VOC to CO ERs are shown as filled traces.
 973

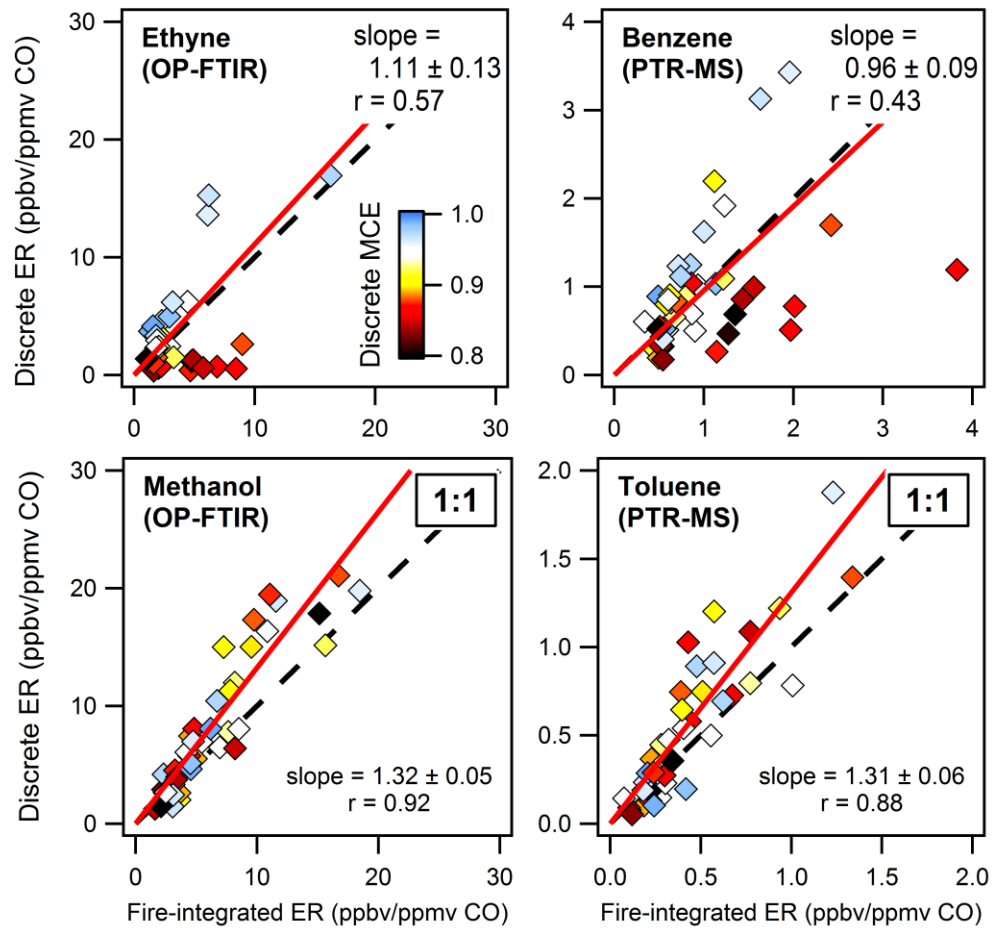


974

975 **Figure 2.** Slopes and correlation coefficients, r , determined from correlation plots of a) mixing ratios
 976 measured by the GC-MS versus the average mixing ratio measured by the OP-FTIR or PTR-MS during
 977 the GC-MS sample acquisition time and b) discrete vs. fire-integrated emission ratios of select VOCs
 978 relative to CO as measured by the OP-FTIR or PTR-MS. The black dashed line represents slopes equal
 979 to 1. The average of the slopes and the standard deviation is shown by the red shaded bands. The
 980 green bands represent $r > 0.90$.

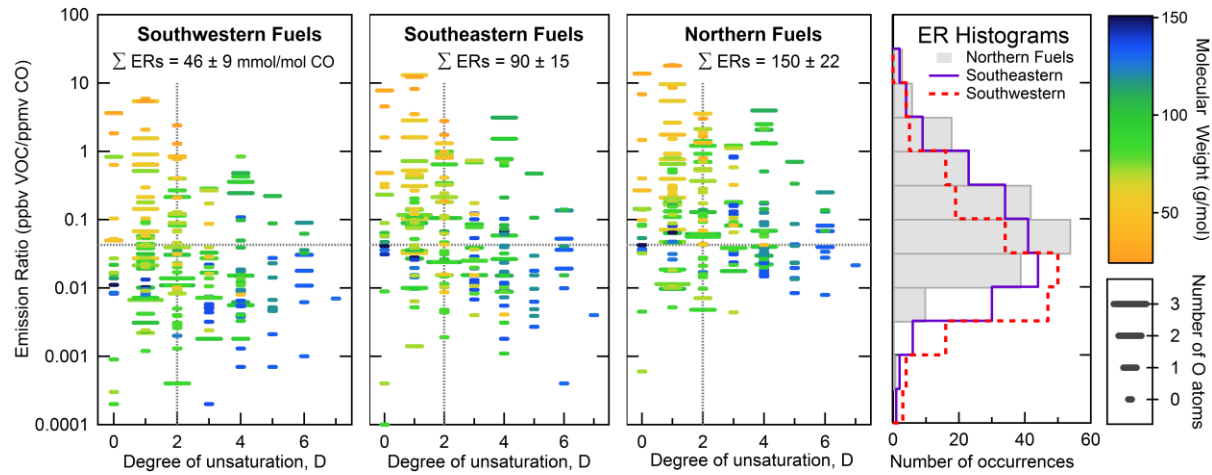


982 **Figure 3.** Correlation plots of the discrete versus fire-integrated emission ratios (ER) for ethyne and
 983 methanol measured by the OP-FTIR and benzene and toluene measured by the PTR-MS. Each data
 984 point represents one biomass burn and are colored by the modified combustion efficiency (MCE)
 985 corresponding to the discrete sampling times of the GC-MS. MCE values near unity are associated with
 986 flaming combustion and lower MCE values are associated with smoldering combustion. The linear 2-
 987 sided regression lines forced through the origin are shown as red lines and the 1:1 ratio is shown by the
 988 dashed lines.



989

990 **Figure 4.** Discrete molar emission ratios for all VOCs reported in Table 2 as a function of the degree of
 991 unsaturation, D, for each fuel region. Emission ratios are colored by the corresponding molecular weight
 992 and the marker width represents the corresponding number of oxygen (O) atoms. The dashed lines
 993 represent the median values for all VOCs from all fuel regions ($ER = 0.0427$ mmol per mol CO and D=2).
 994 The histogram on the right summarizes the distribution of molar emission ratios for each fuel region.

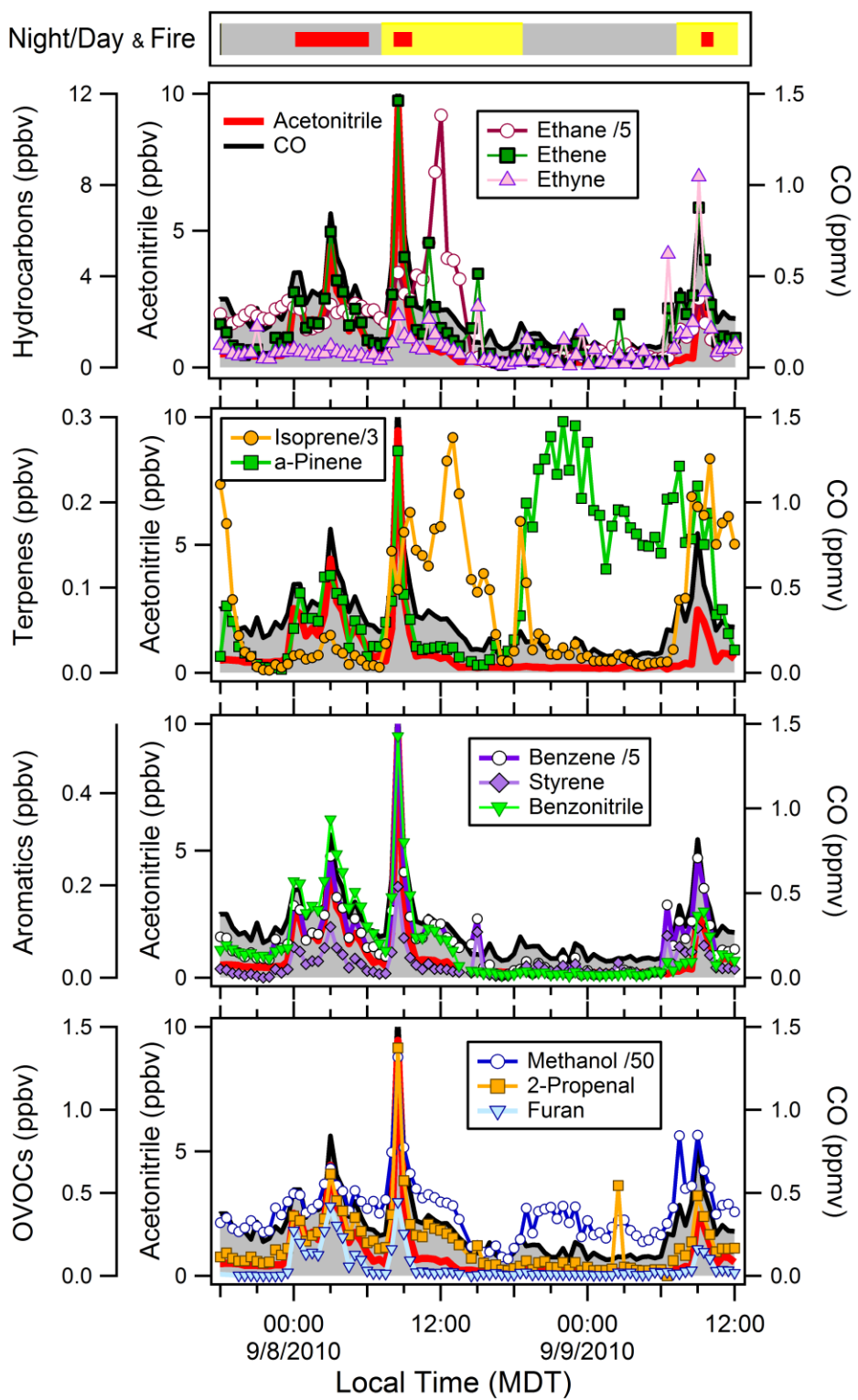


995

996 **Figure 5.** Contributions of (non-methane) VOCs reported in Table 2 to (a-c) the measured molar mass,
997 (d-f) OH reactivity, and (g-i) relative SOA formation potential for the southwestern, southeastern, and
998 northern fuel regions. Totals for each fuel region are shown below each pie chart.

999

1000 **Figure 6.** Time series of ambient air measurements in Boulder, CO during the Fourmile Canyon Fire.
1001 The top bar indicates nighttime (grey), daytime (yellow), and biomass burning plumes (red markers). CO
1002 and acetonitrile are included in all 4 panels.



1004 **Figure 7.** Correlation plots of VOCs versus acetonitrile for all 56 laboratory biomass burns (grey markers)
 1005 and Fourmile Canyon Fire (red markers correspond to the BB plume identified in Fig. 6). The best-fit line
 1006 for the Fourmile Canyon Fire samples is shown in black along with the slope (S) and fit coefficients (r).
 1007

